Analyzer-free, intensity-based, wide-field magneto-optical microscopy

Cite as: Appl. Phys. Rev. **8**, 031402 (2021); https://doi.org/10.1063/5.0051599
Submitted: 26 March 2021 • Accepted: 15 June 2021 • Published Online: 13 July 2021

Rudolf Schäfer, Peter M. Oppeneer, Alexey V. Ognev, et al.

Applied Physics Reviews ARTICLE scitation.org/journal/are

Analyzer-free, intensity-based, wide-field magneto-optical microscopy

Cite as: Appl. Phys. Rev. **8**, 031402 (2021); doi: 10.1063/5.0051599
Submitted: 26 March 2021 · Accepted: 15 June 2021 ·
Published Online: 13 July 2021

Rudolf Schäfer,[1,2,a] Peter M. Oppeneer,[3] Alexey V. Ognev,[4] Alexander S. Samardak,[4,5] and Ivan V. Soldatov[1,b]

AFFILIATIONS

[1]Leibniz Institute for Solid State and Materials Research (IFW) Dresden, Helmholtzstrasse 20, D-01069 Dresden, Germany
[2]Institute for Materials Science, Technische Universität Dresden, D-01062 Dresden, Germany
[3]Department of Physics and Astronomy, Uppsala University, Box 516, SE-75120 Uppsala, Sweden
[4]School of Natural Sciences, Far Eastern Federal University, Vladivostok 690950, Russia
[5]National Research South, Ural State University, Chelyabinsk 454080, Russia

[a]**Author to whom correspondence should be address:** r.schaefer@ifw-dresden.de
[b]Now at Institut für Materialwissenschaft, Technische Universität Darmstadt, D-64287 Darmstadt, Germany.

ABSTRACT

In conventional Kerr and Faraday microscopy, the sample is illuminated with plane-polarized light, and a magnetic domain contrast is generated by an analyzer making use of the Kerr or Faraday rotation. Here, we demonstrate possibilities of *analyzer-free* magneto-optical microscopy based on magnetization-dependent intensity modulations of the light. (i) The transverse Kerr effect can be applied for in-plane magnetized material, as demonstrated for an FeSi sheet. (ii) Illuminating that sample with circularly polarized light leads to a domain contrast with a different symmetry from the conventional Kerr contrast. (iii) Circular polarization can also be used for perpendicularly magnetized material, as demonstrated for garnet and ultrathin CoFeB films. (iv) Plane-polarized light at a specific angle can be employed for both in-plane and perpendicular media. (v) Perpendicular light incidence leads to a domain contrast on in-plane materials that is quadratic in the magnetization and to a domain boundary contrast. (vi) Domain contrast can even be obtained without a polarizer. In cases (ii) and (iii), the contrast is generated by magnetic circular dichroism (i.e., differential absorption of left- and right-circularly polarized light induced by magnetization components along the direction of light propagation), while magnetic linear dichroism (differential absorption of linearly polarized light induced by magnetization components transverse to propagation) is responsible for the contrast in case (v). The domain–boundary contrast is due to the magneto-optical gradient effect. A domain–boundary contrast can also arise by interference of phase-shifted magneto-optical amplitudes. An explanation of these contrast phenomena is provided in terms of Maxwell–Fresnel theory.

I. INTRODUCTION

Numerous applications of the magneto-optical (MO) Kerr effect (MOKE) are well established, including optical magnetometry[1] and magnetic domain imaging in wide-field[2] polarization microscopes[3–5] and by laser-scanning microscopy.[6] All these applications are based on linearly (or plane-) polarized, incident light that—after interaction with the magnetization of the specimen—is transformed into magnetically modulated light on reflection. The reflected light wave may actually be seen as a superposition of a regularly reflected amplitude, $\vec{N}$ (being polarized along the same plane as the incident light, as it would occur in the case of a nonmagnetic material), and a magnetization-dependent Kerr amplitude, $\vec{K}$. The Kerr amplitude is generated by the gyroelectric interaction between the magnetization vector $\vec{m}$ and the electrical field vector $\vec{E}_{\text{in}}$ of the incident light wave, i.e., a nonvanishing cross product, $\vec{m} \times \vec{E}_{\text{in}}$, is required,[3] leading to MO effects that are linear in the magnetization m. This implies constraints for the planes of light incidence and polarization relative to the $\vec{m}$ vector. Three basic Kerr modes are distinguished by convention (Fig. 1):

- *Polar Kerr effect.* Here, the magnetization points along the surface normal, and the effect is strongest (i.e., $\vec{m} \times \vec{E}_{\text{in}}$ is maximal) at perpendicular incidence. The Kerr amplitude is perpendicular to $\vec{N}$, leading to a Kerr rotation by superposition with $\vec{K}$ that is the same for any polarization direction of the incident light.

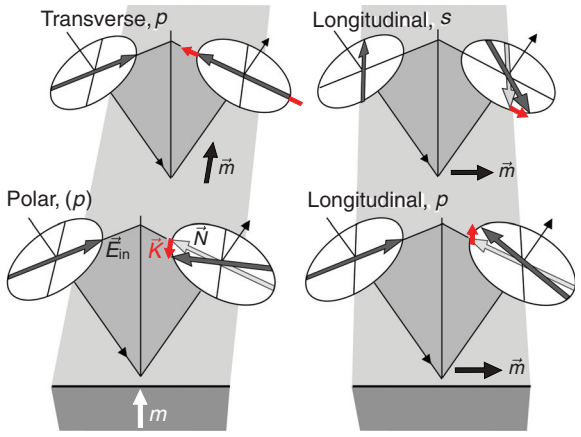

FIG. 1. Schematics of the basic Kerr effect modes. Shown is the magnetization vector ($\vec{m}$), the electrical vector of the incident, plane-polarized light wave ($\vec{E}_{in}$), the regularly reflected field amplitude ($\vec{N}$), and the Kerr amplitude ($\vec{K}$). Inversion of the magnetization direction would lead to an inversion of the Kerr amplitude vectors.

- *Longitudinal Kerr effect*. Oblique incidence of light is required to generate a (detectable) Kerr rotation. Here, the $\vec{m}$ vector lies parallel to the surface and along the plane of incidence. A Kerr rotation is obtained for light that is polarized both parallel and perpendicular to the plane of incidence, called *p*- and *s*-polarized light.
- *Transverse Kerr effect*. Here, the magnetization is in-plane again but perpendicular to the plane of incidence. A Kerr amplitude is generated only for *p*-polarized light (for *s*-polarization, $\vec{m}$ would be parallel to $\vec{E}_{in}$), but its polarization direction is the same as that of the regularly reflected beam.

The same effects are also found in transmission geometry for transparent magnetic specimens, called *Faraday effects*, with one exception: In the transverse configuration, no (linear–in-$\vec{m}$) MO effect is possible in transmission because the cross product is either zero or points along the propagation direction, thus making an MO Faraday amplitude, $\vec{F}$, impossible. The Faraday signal is normally much stronger than the corresponding Kerr signal because the light interacts with the magnetization across the whole specimen thickness and not just within some penetration depth as for the Kerr effects. Faraday microscopy is also possible in reflection geometry if the transparent sample is placed or deposited on a mirror.

In the case of the rotational effects, a detectable magneto-optical signal or domain contrast is finally obtained by using an analyzer in the reflection (or transmission) path that blocks the emerging amplitude differently for differently magnetized domains, resulting in a magnetization-dependent intensity modulation of the reflected (or transmitted) light. If there is a phase shift between $\vec{N}$ and $\vec{K}$ (or $\vec{F}$), the rotated light will also be elliptically polarized, requiring a phase shifter (called a compensator) for contrast optimization.[7]

The Kerr and Faraday effects are characterized by the fact that they are all, to the lowest order, linear in the local magnetization *m*. Two other effects[7] can lead to MO contrasts by using plane-polarized light in an optical polarization microscope. The *Voigt effect* depends quadratically on the magnetization and, consequently, generates a contrast between domains that are magnetized in-plane and along different *axes* rather than directions. As the light, emerging from the specimen, is predominantly elliptically polarized in the case of the Voigt effect, the use of a compensator is mandatory in order to generate a detectable rotation. The MO *gradient effect*, finally, is a birefringence effect that depends linearly on gradients in the magnetization vector field.

Apart from the well-known Kerr and Faraday *rotation*, MO effects can also manifest themselves as a magnetically induced modification of the light's *amplitude* in either transmission or reflection geometry.[8] One such example is the aforementioned transverse Kerr effect. As the transverse Kerr amplitude is polarized along the same plane as the regularly reflected beam (compare Fig. 1), the transverse Kerr effect causes an amplitude variation of the light rather than a rotation. Another prominent example is the magnetic circular dichroism (MCD) effect, which is customarily observed in transmission through a magnetic sample (see, e.g., Ref. 9). In the x-ray regime, magnetic imaging using the x-ray magnetic circular dichroism (XMCD) has been successfully applied in a transmission soft x-ray microscope[10] and in combination with photoexcitation electron emission microscopy (PEEM),[11,12] which both permit visualization of submicrometer-sized ferromagnetic domains. The x-ray magnetic linear dichroism (XMLD) is a MO effect related to the Voigt effect that has been used to image antiferromagnetic domains in combination with PEEM.[13,14] These magnetic dichroic effects can be observed as well in a photon-in–photon-out reflection experiment when using circularly or linearly polarized x rays (see, e.g., Refs. 15 and 16). The appearance of these MO effects as an amplitude variation is thus distinct from those characterized by a MO rotation, but all MO effects can be described within the common Maxwell–Fresnel framework.[8,17] This, therefore, raises the question of whether also the amplitude-modulation effects can be used for magnetic imaging at visible frequencies and which method is optimally suited.

Thus far, *rotation-based* Kerr, Faraday, and Voigt microscopy have been (almost) exclusively employed for domain imaging in the visible frequency regime.[3–5] A recent investigation[18] on ultrathin magnetic films showed that antireflection coatings could significantly enhance the MO rotation and further found that a MO contrast could even be detected by illuminating the sample with left- and right-circularly polarized (LCP and RCP) light rather than by plane-polarized light, thus, indeed, making use of the MCD effect. The latter contrast was enhanced by the extreme antireflection coating used in that work, but it indicates the possibility of magnetic domain imaging without the need for an analyzer, which would not have any effect on a circularly polarized wave anyway. In another recent article[19] the MCD effect was employed as well to image domains on an ultrathin, two-dimensional $CrBr_3$ magnetic film at low temperature; however, the ultrathin film was illuminated with plane-polarized light, and the MCD signal was extracted after reflection by using a quarter-wave plate and an analyzer. Again, the Kerr signal was significantly enhanced by interference effects with an underlayer resembling the mentioned antireflection effect. Interestingly, the magneto-optics of $CrBr_3$ material (on bulk crystals, though) was already investigated back in the 1960s.[20,21] In 1975, Kuhlow and Lambeck[22] published domain images of a 12-μm-thick $CrBr_3$ single crystal, imaged in blue, *circularly polarized* light by Faraday microscopy at 15 K. To our best

knowledge, this is the first wide-field microscopic observation of magnetic domains making use of the MCD effect in the absence of an analyzer. Noteworthy is also a recent article[23] in which an alternative microscopy technique was introduced. There, the MCD effect was combined with the Seebeck effect in a ferromagnet–semiconductor bilayer, thus detecting the MCD signal electrically in a transmission geometry.

From an application-oriented perspective, *establishing* analyzer-free magnetic microscopy could be advantageous as it reduces the need for the extra optical element, provided that the magnetic modulation of the amplitude is large enough. Since these various MO effects can all be described within the Maxwell–Fresnel framework, it can be anticipated that those based on intensity modulation can indeed be employed for magnetic microscopy, given an appropriate measurement geometry, even without antireflection coating.

In this article, we review several possibilities for analyzer-free MO wide-field microscopy making use of intensity-modulated light. To provide the basics, we will start with the theory of the MO effects in Sec. II, followed by some experimental details (Sec. III) and a section that briefly recaps conventional, analyzer-based Kerr microscopy for comparison (Sec. IV). In Sec. V, we then show that the amplitude modulation of linearly polarized light due to the transverse Kerr effect can well be employed for magnetic domain imaging. In Sec. VI, we report on the identification of one further MO intensity modulation configuration that is suitable for direct MO imaging when employing plane-polarized light for illumination. In Secs. VII, VIII, and IX we demonstrate that magnetic microscopy is also possible by illuminating the magnetic specimen with circularly polarized light, i.e., by making direct use of the MCD effect similar to XMCD.[7,11,24,25] Not only is this feasible for perpendicularly magnetized films with sophisticated antireflection coatings as mentioned but also works for both in-plane and perpendicular media, even in the absence of antireflection coatings. In Sec. X, we demonstrate that the MLD effect also leads to a domain contrast, which is superimposed by a domain boundary contrast due to the magneto-optical gradient effect. To check for eventualities, we have examined the existence of contrasts in a different microscope type with separated illumination and reflection paths (Sec. XI). At the end of the paper (Sec. XII), we finally mention three further aspects that might be worth examining in future work. These include (i) the influence of the light color on various Kerr contrasts, (ii) the finding that a domain contrast can even be seen in the absence of analyzer *and* polarizer, and (iii) diffraction effects at domain boundaries. In this context, we also refer to largely forgotten, 60-year-old research that already pointed out the possibility of magneto-optical imaging without the need of a polarizer and analyzer but, however, based on dark-field optical microscopy.[26]

II. THEORY

The here-studied Kerr and Faraday effects are characterized by the fact that they are all, to the lowest order, linear in the local magnetization m and can all be described on the same footing within the macroscopic Maxwell–Fresnell theory.[8,17,27] In this formulation, the complex Voigt constant Q_V ($\sim m$) captures the MO interaction strength of the Kerr and Faraday effects.

To start with the MO *rotation* effects, these can be understood by applying a concept that was originally proposed by Fresnel to describe optical activity:[17] A plane-polarized light wave can be represented by the superposition of LCP and RCP partial waves with the same amplitudes. By solving the Fresnel wave equation for ferro- or ferrimagnetic materials, only two such circularly polarized eigenmodes with opposite rotation sense can propagate *along* the magnetization vector within the material. A plane-polarized wave entering the material is thus resolved into these two eigenmodes (Fig. 2). Each mode experiences its own (complex) index of refraction, n_{RCP} or n_{LCP}, during propagation. The difference of the indices is $n_{RCP} - n_{LCP} \approx -\bar{n} Q_V$, with $\bar{n}$ being the average index of refraction. The two partial waves will hence advance with different velocities and amplitudes in the material. The former result in a phase shift, which leads to a rotated plane wave by superposition of the two partial waves, the rotation sense of which depends on the magnetization direction [Fig. 2(a)]. The Faraday rotation θ_F is thus proportional to $\mathrm{Re}[n_{RCP} - n_{LCP}]$. The same concept applies to the Kerr effect in reflection. The Kerr and Faraday rotations can therefore be equally regarded as *circular birefringence* effects, i.e., a birefringence of circularly polarized light. The difference in absorption conversely causes different amplitudes of the two circular modes [Figs. 2(b) and 2(c)], which in transmission leads to *circular dichroism* in Fig. 2(c) and elliptically polarized light by superposition in Fig. 2(b), where the Faraday ellipticity is proportional to $\mathrm{Im}[n_{RCP} - n_{LCP}]\ \mathrm{Im}[n_{RCP} - n_{LCP}]$. Note that these refractive indices are different when $(\vec{k} \cdot \vec{m}) \neq 0$, $\vec{k}$ is the wave vector of the light, thus when there is a component of m along the propagation direction.

In Sec. I, we have seen that in the case of the rotational effects, a domain contrast is obtained by using an analyzer and possibly a compensator in the reflection (or transmission) path that blocks the emerging amplitude differently for differently magnetized domains, thus causing a magnetization-dependent intensity modulation of the reflected (or transmitted) light. In the case of pure Kerr (or Faraday) ellipticity [Fig. 2(b)], a domain contrast cannot be generated by an analyzer alone due to the elliptical character of the light (analyzer *and*

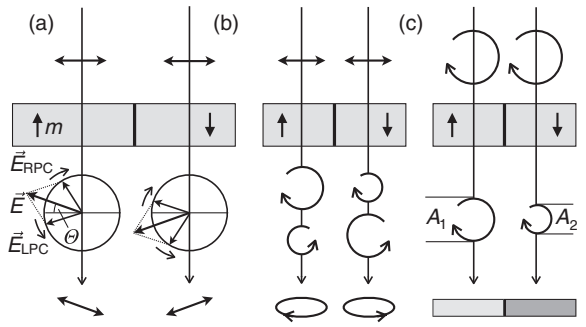

FIG. 2. (a) Schematic representation of magnetic circular birefringence or Faraday effect: Plane-polarized light is resolved into left- and right-handed circular partial waves that are phase shifted, resulting in rotated plane waves dependent on the magnetization direction. (b) Different damping of the two partial wave amplitudes, which is inverted by inverting the magnetization direction, results in elliptical waves with opposite handedness (Faraday ellipticity). Note that the effects of (a) and (b) generally occur together so that the emerging light is usually rotated *and* more or less elliptically polarized. (c) MCD for the case of right-handed circular illumination. Differential, magnetization-dependent damping of the circular wave leads to absorption domain contrast. The effects are shown for transmission (Faraday) geometry, but they similarly apply to reflection (Kerr) geometry.

compensator would be required to transform the two ellipses into a detectable rotation). Instead, one can exploit the (normalized) MCD intensity difference [Fig. 2(c)],

$$A_C = \frac{I_{RCP} - I_{LCP}}{I_{RCP} + I_{LCP}} \propto \mathrm{Im}[n_{RCP} - n_{LCP}] \tag{1}$$

of the transmitted intensities I_{RCP} and I_{LCP}, which does not require an analyzer or compensator.

For the transverse Kerr effect $(\vec{k} \cdot \vec{m}) = 0$, the refractive indices do not depend on m in linear order. The effect instead results in the aforementioned amplitude modulation for which an analyzer would as well be useless. This effect is therefore mainly applied in MOKE magnetometry for measuring purposes by using a photodetector.[28,29] Also, domain imaging under pure transverse conditions has been demonstrated by sequentially building up an image from laser-illuminated spots in a scanning Kerr microscope.[30] For wide-field Kerr microscopy, however, the transverse Kerr effect has so far only been applied[31] as a "rotational" effect by polarizing the light at 45° to the plane of incidence. Then the perpendicular light component is not affected by the magnetization, while the parallel component receives an amplitude modulation leading to a detectable rotation in the superposition of the two components.[32]

The reflection MO effects that appear as a magnetic intensity modulation can be described by the reflection matrix coefficients for s- and p-polarized light

$$\vec{E}_{out} = \mathbf{r} \cdot \vec{E}_{in}, \tag{2}$$

with $\vec{E}_{in} = (E_s, E_p)$. The 2×2 matrix $\mathbf{r}$ depends on the magnetization $\vec{m}$ and can be written in Jones' notation as

$$\mathbf{r} = \begin{pmatrix} r_{ss} & \Delta_{sp} \\ \Delta_{ps} & r_{pp} + \Delta_{pp} \end{pmatrix}. \tag{3}$$

Here, r_{ss} and r_{pp} are the standard, nonmagnetic (Fresnel) reflection coefficients for s- and p-polarized light, whereas the coefficients Δ_{sp}, Δ_{ps}, and Δ_{pp} depend linearly on $\vec{m}$. One can utilize the three orthonormal directions of the geometry to define the transverse m_T, longitudinal m_L, and polar m_P magnetization components, respectively, such that $\vec{m} = (m_T, m_L, m_P)$.[8] The coefficient Δ_{pp} depends on m_T only, whereas Δ_{sp} and Δ_{ps} depend on both m_L and m_P.[27]

The transverse Kerr effect appears as a magnetic change in the reflected intensity caused by Δ_{pp}. The corresponding asymmetry is given as

$$A_T = \frac{R_p(+m_T) - R_p(-m_T)}{R_p(+m_T) + R_p(-m_T)}, \tag{4}$$

with $R_p = |r_{pp} + \Delta_{pp}|^2$; using the expressions for r_{pp} and Δ_{pp} (see Ref. 27), it can be shown that $A_T \propto Q_V$.[8] It deserves to be mentioned at this point that A_T can equally well be measured with linearly *and* circularly polarized $[\vec{E}_{in} = \frac{1}{\sqrt{2}}(1, \pm i)E_0]$ light, and even unpolarized light, as long as there is a nonzero E_p component.

For a longitudinal magnetization, it is possible to observe a dichroic reflectivity contrast under specific conditions. First, using LCP and RCP radiation, a magnetic asymmetry exists, given by

$$A_L^C = \frac{R_{RCP} - R_{LCP}}{R_{RCP} + R_{LCP}}, \tag{5}$$

which is proportional to $\Delta_{sp} \propto Q_V$.[15] A consequence of the similarity with Eq. (4) is that when the magnetization vector is rotated in-plane from the transverse to the longitudinal direction, the contrast recorded with circularly polarized light will additively contain A_T and A_L and change goniometrically between these two.

Second, using linearly polarized light, it is possible to measure a longitudinal dichroic reflection contrast as well.[33,34] This rather unknown MO effect is maximal when the incoming light is plane-polarized at an angle θ of 45° with respect to the incidence plane, but it exists also for other angles θ. It becomes maximal when the magnetization direction is reversed in an applied field or when measuring antiparallel domains, and is expressed as $A_L^L = [R_\theta(+m_L) - R_\theta(-m_L)]/[R_\theta(+m_L) + R_\theta(-m_L)]$. Explicit expressions were given previously and show that $A_L^L \propto Q_V \sin 2\theta$.[34] Consequently, this provides a second option to measure magnetic intensity contrast using linearly polarized light. For convenient use, this dichroic contrast can be reformulated by using $R_\theta(+m_L) + R_\theta(-m_L) \approx 2R_\theta(0) \approx 2R_{-\theta}(0)$, with $R_\theta(0)$ being the reflectivity of the nonmagnetized material. Further, using that inverting the magnetization $\vec{m}$ is equivalent with changing θ to $-\theta$ (see Ref. 34), one can rewrite A_L^L as

$$A_L^L \approx \frac{R_\theta(m_L) - R_\theta(0)}{2R_\theta(0)} - \frac{R_{-\theta}(m_L) - R_{-\theta}(0)}{2R_{-\theta}(0)}. \tag{6}$$

In this MO effect, a maximum contrast appears for longitudinal domains at oblique incidence when contrasts for $\theta = 45°$ and $-45°$ are subtracted. Even without subtraction, each of the terms in Eq. (6) already provides a contrast, but with an opposite sign. At normal incidence, the longitudinal contrast vanishes. It deserves to be mentioned that for a *polar* out-of-plane magnetization, an equivalent magnetic dichroic effect, A_L^P, in reflection exists,[34] which should thus as well be suitable for magnetic imaging of such domains. Alternatively, the MCD in reflection can be used to image out-of-plane magnetizations.

To summarize, using plane-polarized light, one can thus detect magnetic contrast as an amplitude modulation, using either A_T, A_L^L, or A_L^P, depending on the direction of the domain magnetization. The magnitude of contrast will vary with the angle between the light's polarization and incidence plane and also with the direction of the magnetization with respect to the principal orthonormal directions (i.e., polar, longitudinal, and transverse). A further option is to use circularly polarized light and the MCD in reflection that can be employed to image in-plane and out-of-plane magnetic domains when there is a component of the magnetization along the wave vector, i.e., $(\vec{k} \cdot \vec{m}) \neq 0$.

At the end of this paper, we will show that besides the so-far discussed MO effects that are all linear in the magnetization, the (quadratic) Voigt effect can also be employed for analyzer-free domain imaging. This effect, which can be applied in transmission[35] as well as in reflection geometry[36] and which was also found in the x-ray regime,[16] occurs when the light propagates transverse to the magnetization vector. Here, the eigenmodes are two *linearly* polarized waves with vibrational planes along and perpendicular to $\vec{m}$. Incident light,

plane polarized along one of these two directions, will thus not alter its polarization in the magnetic medium. If the polarization plane is at an angle to $\vec{m}$, however, the polarization state will be changed, with the strongest effect occurring at an angle of 45°. This is due to the fact that both linear eigenmodes are experiencing different refractive indices $n_{\parallel}$ and $n_{\perp}$ so that they proceed in the medium with different velocities and with different attenuations. The light thus experiences a magnetic linear birefringence proportional to $\mathrm{Re}[n_{\parallel} - n_{\perp}]$ and a magnetic linear dichroism proportional to $\mathrm{Im}[n_{\parallel} - n_{\perp}]$ (note that here, the word "linear" refers to the polarization mode of the light and not to the order of the effect). In the case of linear birefringence, the two partial waves are retarded relative to each other so that the outgoing light is elliptically polarized with a handedness that depends on the relative orientation of the polarization plane and magnetization axis. Oppositely magnetized domains, following the same axis, can therefore not be distinguished in their birefringence effect. MLD results in a rotation of the emerging light due to the different amplitudes of the partial wave. Note that the phenomenology is thus *opposite* to that of magnetic circular birefringence and dichroism, where birefringence causes a rotation and dichroism leads to ellipticity[37] (compare Fig. 2).

While conventionally the ellipticity of light due to the Voigt effect is transformed into linearly polarized light by a compensator and then brought to a contrast with the help on an analyzer,[7] it can be expected that the selective amplitude modulation due to the MLD effect can directly lead to an MO contrast as will be demonstrated in Sec. X.

III. EXPERIMENTAL

Most of the presented domain images have been obtained in a wide-field optical polarization microscope (Carl Zeiss Axioscope) with Köhler illumination scheme[5] [Fig. 3(a)]. The light of four light-emitting diodes (LEDs) is guided to the lamp house by fiberoptics.[38,39] The ends of the fibers are physically located at a plane that is confocal with the back focal plane of the objective lens. By a beam splitter, consisting of a semipermeable mirror at an orientation of 45° to the incoming ray path, the light is deflected downward to the objective lens [Fig. 3(c)]. After reflection from the sample, the light passes the mirror again on its way toward the camera or oculars. A centered fiber would result in a perpendicular incidence of light, while off-centered fibers would lead to an oblique incidence with two orthogonal planes that can be chosen by activating one of the four LEDs [in Fig. 3(c), this is illustrated for LED-1; the angle of incidence was ∼30° for all four LEDs]. By alternately pulsing two LEDs synchronously with the camera exposure, two Kerr modes can quasi-simultaneously be run, and the corresponding images can be displayed.[39,40] Note that in the beam splitter, only plane-polarized light along the x and y axes is reflected linearly toward the sample; for other orientations, the light hitting the sample is elliptically polarized. Either white, red (640 nm), or blue (450 nm) LED light was used as indicated in the figure captions. A 20×/0.5 (magnification/numerical aperture) objective lens was used for all experiments in the wide-field microscope.

Circularly polarized light was generated by using a rotatable linear foil polarizer followed by a quarter-wave plate [Fig. 3(b)] that was placed right on the entry side of the beam splitter. The fast axis of the quarter-wave plate was aligned diagonally at 45° to the x and y axes. Setting the polarization plane then along the x and y axes results in RCP and LCP polarized light, respectively. Two quarter-wave plates were applied: One plate, designed for a wavelength of 635 nm, was

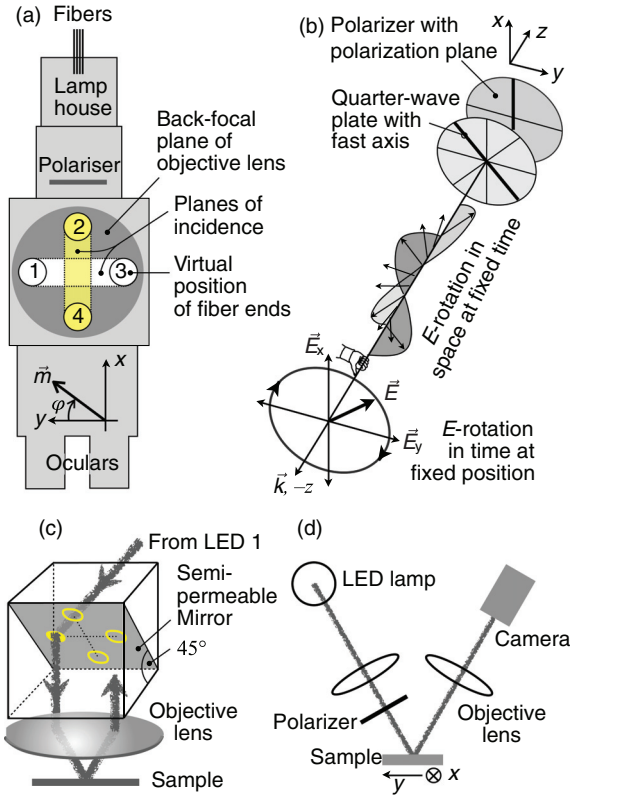

FIG. 3. (a) Schematic top view of our wide-field Kerr microscope, emphasizing the two orthogonal planes of incidence that can be chosen by the activation of proper LEDs. The polarizer, sitting in the illumination path, is by standard linear but can optionally be replaced by a circular polarizer. The analyzer (not shown) is located behind the objective on the reflection path. Indicated is the coordinate system to define the plane of incidence and the magnetization direction. In the upcoming figures, we will refer to this coordinate system and the given LED numbers. (b) Generation of (right-handed) circularly polarized light by a linear polarizer and a quarter-wave plate. Rotating the polarizer by 90° would result in left-handed circular light. (c) Semipermeable reflector plate (beam splitter), sitting in the illumination path above the objective lens. Illustrated is the ray path for light from LED-1. (d) Schematics of a simple Kerr microscope with separated illumination and reflection paths, which we have optionally used for selected experiments.

used for investigations with red LED light, while another, designed for a wavelength of 550 nm (green light), was employed for white and blue light.[41] For the second case, it is expected that the light is strongly elliptically polarized rather than circular. Unless mentioned otherwise, imaging was performed in reflection geometry without an analyzer. To prevent overexposure of the camera, the intensity of the LEDs (which under regular Kerr conditions need to be maximized) had to be dimmed by a gray filter in the illumination path.

Most experiments were performed on an ideally oriented grain of a Fe-3 wt. %-Si sheet, with cube texture being characterized by a (100) surface with two easy axes of anisotropy parallel to the surface.[3] The specimen was coated with a zinc-sulfide antireflection layer to enhance the Kerr effect.[42] A circular piece of such a 0.5-mm-thick sheet with a diameter of 10 mm was placed between the pole pieces of a quadrupole

TABLE I. Summary of investigated samples. Listed is the wavelength of the applied LED light, the wavelength for which the quarter-wave plate is optimized, and the figure numbers in which the specimens are imaged.

Sample	FeSi					Garnet		CoFeB	Pt/Co/Pt
Wavelength, nm	640	640	640	450	White	640	640	White	White
Quarter-wave plate, nm	—	635	550	550	550	—	635	550	550
Figure number	4, 5, 7, 13, 14, 16, 17	8, 9	14, 16	16	16	10, 11, 14, 18	10, 15	12	14

electromagnet that allows for a computer-controlled rotation of the field by 360°. "Kerr-sensitivity" curves were measured by plotting the image intensity of a freely selectable sample area in the saturated sample state as a function of magnetic field direction. The field direction thus corresponds to the magnetization direction defined by the angle φ [see Fig. 3(a)]. All sensitivity curves were recorded on the unprocessed microscope image with the background image intensity adjusted to the same value by tuning the LED intensity. All domain images shown on the FeSi material are difference images in which a background image of the saturated state is subtracted to digitally enhance the contrast.[43]

For polar Faraday studies, a magneto-optical indicator film (MOIF) with perpendicular anisotropy was used as the sample. The MOIF, provided by Matesy GmbH,[44] consists of a magnetic garnet film deposited on a transparent gadolinium–gallium–garnet (GGG) substrate and covered by a thin mirror layer. Polarized light enters the MOIF, passes the substrate and the magnetic film, and is then reflected from the mirror, thus passing the magnetic film twice. In the magnetic garnet film, a Faraday rotation is induced, which depends on the local magnetization of the film, and that is actually doubled due to the double penetration and the nonreciprocity of the Faraday rotation. The garnet film of the MOIF stack is thus effectively studied in transmission in a reflection polarization (Kerr) microscope. "Real" polar *Kerr* microscopy was applied to an ultrathin cobalt–iron–boron single-layer film (0.9 nm thick) and to a Pt (3 nm)/Co (1 nm)/Pt (3 nm) film, both with perpendicular anisotropy and not covered by antireflection coatings. All investigated samples are collected in Table I, showing the wavelength of the light and possibly the quarter-wave plate that have been used together with the figures in which images of the specimens appear throughout the paper.

To check for eventualities, selected experiments have been performed in a homemade microscope with separated illumination and reflection paths [Fig. 3(d)]. The lateral resolution of this setup is only of the order of 30 μm,[45] it only allows for oblique incidence at a fixed angle of 30°, but it has the advantage that the polarized light *directly* hits the specimen without the need of a beam splitter.

IV. CONVENTIONAL LONGITUDINAL KERR MICROSCOPY

To better understand the peculiarities of the analyzer-free contrast phenomena in our FeSi material, let us briefly recap the typical domain contrast and sensitivity curves in conventional, analyzer-based longitudinal Kerr microscopy. For the experiments on this material, *red* light was used because it provides the best domain contrast; we have measured that blue and white light only lead to maximum longitudinal contrasts of 46% and 51%, respectively, of that of red light. Such a trend is expected from the Kerr spectra of iron.[8] As the best (obtained) contrasts of all sensitivity curves in this paper are below the maximum longitudinal Kerr contrast in red light, we have used that contrast $C_{\mathrm{max}}^{\mathrm{long}}$ as reference. For each sensitivity curve presented here, we have calculated the contrast by $C = (I_2 - I_1)/(I_2 + I_1)$ with I_2 and I_1 being the maximum and minimum intensities, respectively, when turning the magnetization in the range of 360°. Throughout this paper, all given Kerr intensities are normalized to $C_{\mathrm{max}}^{\mathrm{long}}$, which allows comparison of the "strengths" of all reported effects.

In Fig. 4, two complementary domain images and sensitivity curves are shown, which were obtained with red LED-3 and -4, i.e., at orthogonal planes of incidence. The polarizer was fixed along the y axis in both cases, so the light from LED-3 hits the sample in the

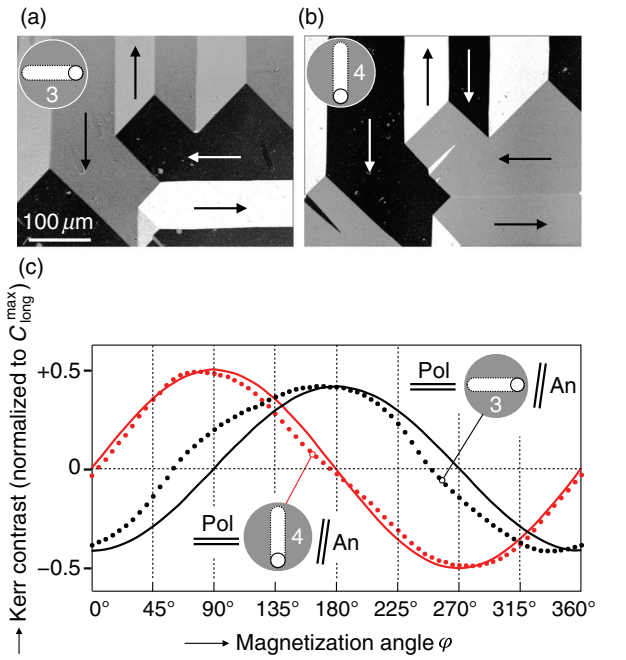

FIG. 4. Domains (a, b) and sensitivity curves (c) on our FeSi sample, recorded by the conventional longitudinal Kerr effect using an analyser in the reflection path of the microscope that was opened by an angle of 8° relative to the axis perpendicular to the polariser axis. Red LEDs at positions 3 and 4 were used, and the polarizer was along the y axis, leading to *p*- and *s*-polarized light, respectively. The dotted curves are measured, while the full-line curves are regular sine and cosine functions to guide the eye. Due to a superimposed transverse Kerr effect in the case of *p*-polarization, the two curves are phase shifted by <90°. The arrows in the domain images indicate the magnetization directions, which strictly follow the two orthogonal easy axes. The maximum contrast of the sensitivity curves, shown in this plot, is used for normalizing all intensities throughout the paper.

p-polarized state, whereas it is *s*-polarized for LED-4, corresponding to the two longitudinal cases in Fig. 1. While the domain contrast transverse to the plane of incidence disappears for LED-4 as expected for longitudinal Kerr sensitivity [Fig. 4(b)], there is considerable transverse contrast for LED-3 [Fig. 4(a)]. This is also visible in a notable phase shift of the corresponding sensitivity curve in Fig. 4(c). Here also, $\sin\varphi$ and $-\cos\varphi$ functions are plotted that should ideally be measured under *pure* longitudinal sensitivity conditions to better see the apparent deviations between measured and ideal curves. In Ref. 46, we have thoroughly investigated this effect, proving that it is caused by an intensity modulation of the reflected light due to the transverse Kerr effect, which is superimposed on the longitudinal rotation effect that primarily determines the contrast. As explained in Fig. 1, a transverse Kerr effect is only expected for *p*-polarized light in accordance with the findings in Fig. 4.

Besides the phase shift of the sensitivity curve measured with *p*-polarization, both curves in Fig. 4 are more or less distorted. This indicates that besides the transverse Kerr effect, other intensity-modulation effects might be superimposed; in the remainder of this paper, several such effects will be identified. Such curve distortions need also to be considered when sensitivity curves are used to calibrate the domain intensity for quantitative Kerr microscopy.[31,47] Just recording the intensity at field angles that are multiples of 45° and assuming that the intensity is a strictly linear function of the longitudinal and transverse magnetization components (as suggested in Ref. 31) may be dangerous. It is furthermore worth notice that the curve distortions can be strongly reduced[46] by running the microscope in the pure longitudinal mode,[39] i.e., by pulsing opposite LEDs in synchronization with the camera and subtracting the two pictures.

V. TRANSVERSE KERR MICROSCOPY

In Sec. IV, we have seen that the conventional longitudinal Kerr contrast, obtained by the use of an analyzer, can be modulated by a superimposed transverse Kerr effect that leads to a phase shift of the otherwise longitudinal sensitivity curve. By choosing *p*-polarized light and removing the analyzer, the conditions are ready to measure the *pure* transverse Kerr effect. An intensity modulation of the reflected light is then expected that depends on the magnetization direction of an in-plane magnetized specimen (compare Fig. 1). While *quasi-transverse* imaging at 45° polarization is well established as mentioned in Sec. I, wide-field Kerr microscopy under *pure transverse* conditions has not yet been published to the best of our knowledge. This is somewhat surprising because a pure transverse domain contrast can well be seen as demonstrated in Fig. 5. Enhanced by background subtraction, the contrast is even of comparable strength as that of conventional, longitudinal Kerr microscopy.

The contrast symmetry corresponds to expectations: By comparing Figs. 5(a) and 5(b), it is obvious that the domain contrast transverse to the plane of incidence is inverted when the direction of incidence is inverted due to an inverted cross product $\vec{m} \times \vec{E}_{\mathrm{in}}$ [see also Eq. (4)]. This domain contrast disappears when the plane of incidence and the polarizer are rotated by 90° [Fig. 5(c)], consistent with the vanishing transverse Kerr effect A_{T} for a longitudinal magnetization, and the longitudinal effect $A_{\mathrm{L}}^{\mathrm{L}}$ also vanishes for $\theta = 0$. Now the horizontal domains are transverse to the plane of incidence, thus showing up with maximum contrast. If the light is polarized orthogonal to the plane of incidence [i.e., *s*-polarized as shown in Fig. 5(d)], no

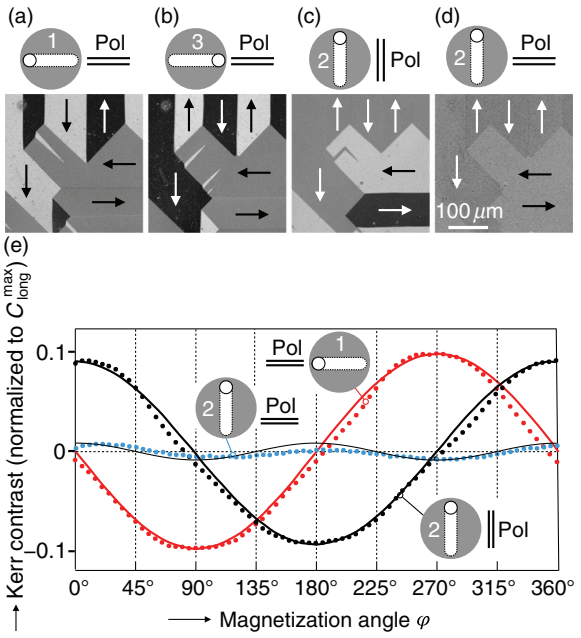

FIG. 5. Analyzer-free Kerr microscopy under pure transverse conditions, again by using red light. The domain images in (a)–(d) were obtained on the FeSi sheet under the indicated conditions, e.g., in (a), the sample was illuminated by LED-1 and the light was *p*-polarized, while for (b) the direction of incidence was inverted under the same polarization. The plots in (e) show the Kerr sensitivities for three cases. To guide the eye, $\cos\varphi$, $-\sin\varphi$, and $\cos 2\varphi$ functions have been added as they are expected to be measured under "ideal" conditions. The contrast is normalized to $C_{\mathrm{max}}^{\mathrm{long}}$, i.e., the maximum contrast that was achieved under conventional, longitudinal conditions (compare Fig. 4).

domain contrast would be expected at all as now the Kerr amplitude either vanishes for transverse magnetization components, i.e., along the polarizer axis, or a nonvanishing Kerr amplitude will appear for rotated magnetization, which, however, leads to a longitudinal *Kerr rotation* that cannot be detected without an analyzer. Nevertheless, a weak domain contrast appears in Fig. 5(d) that is *quadratic* in the magnetization. It is characterized by antiparallel domains of the same color and a contrast between domains magnetized at 90°. In Sec. X, we will address this quadratic contrast phenomenon again, showing that it is caused by the MLD effect. If the domains in Fig. 5(d) would be imaged under the same conditions but with an analyzer added, the vertical domains would show up with maximum contrast due to the aforementioned longitudinal Kerr rotation.

The sensitivity curves in Fig. 5(e) confirm this contrast phenomenology. For *s*-polarized light, a curve with low contrast of just 2% of $C_{\mathrm{max}}^{\mathrm{long}}$ is measured. It can well be approximated by a quadratic $\cos 2\varphi$ function. For *p*-polarization, sinusoidal intensity dependencies are measured with (approximate) zero crossings whenever the magnetization is parallel to the plane of incidence. Turning the plane of incidence together with the polarizer by 90° results in a phase shift of the sensitivity function by ~90°, i.e., only the component of magnetization perpendicular to the incidence plane results in a variation of the reflected light intensity as expected for the transverse Kerr effect. Compared to the sensitivity curves in Fig. 4, the maximum contrast of

the transverse curves is only 20% of C_{max}^{long}, but they are significantly less disturbed.

VI. LONGITUDINAL 45°-DICHROIC KERR MICROSCOPY

In Sec. II, we introduced a longitudinal dichroic reflection effect that is expected to occur by using linearly polarized light like for the transverse Kerr effect. The longitudinal contrast should be maximum at a polarization angle of 45° with respect to the plane of incidence. Under this condition, the incoming light has both *s*- and *p*-polarization components. For a longitudinal magnetization, the reflected electric field components $E_{out,s,p}$ of the *s*- and *p*-polarized components are altered by the magnetic reflection coefficient Δ_{sp}, leading to a changed intensity of the reflected light. Note that when the magnetization is rotated, the *p*-polarized component should also cause a transverse Kerr effect that should be superimposed on this longitudinal dichroic effect.

The contrast phenomenology of the longitudinal dichroic effect can be visualized by applying the Lorentz concept like in Fig. 1. In Fig. 6, this is illustrated for two polarizer settings at ±45° relative to the plane of incidence and a given longitudinal magnetization direction. The *s*- and *p*-components of the incoming electric field vector $E_{in,s,p}$ are responsible for the indicated Kerr vectors $\vec{K}_{s,p}$ on the reflection paths. By vector addition with the normally reflected light vector $\vec{N}$, this results in an extension [Fig. 6(a)] or shortening [Fig. 6(b)] of the outgoing field vector $\vec{E}_{out}$, i.e., an increase or decrease in the total reflected amplitude when the polarizer is turned from +45° to −45°. Turning the magnetization by +180° (not shown) will lead to inverted Kerr vectors and thus to inverted reflected light amplitudes. The domain contrast will consequently change sign when turning the polarizer from +45° to −45°.

In fact, we were able to identify this predicted effect and its superposition with the transverse Kerr effect as demonstrated in Fig. 7. Turning the polarizer to ±45° leads to sensitivity curves that are phase shifted by approximately ±45° compared to those of the pure transverse or pure longitudinal effects [compare the curves in Figs. 7(i) and 7(j) with those in Figs. 4 and 5]. This indicates that the transverse and

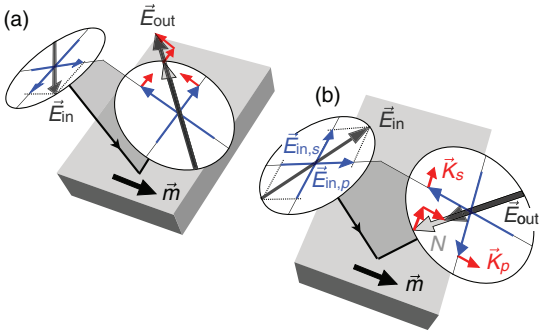

FIG. 6. Lorentz concept of the longitudinal 45°-dichroic Kerr effect. Shown are the electrical field vectors of the illuminating light ($\vec{E}_{in}$), the normally reflected light ($\vec{N}$), the Kerr amplitude ($\vec{K}$), and the totally reflected light ($\vec{E}_{out}$). The *s*- and *p*-components of the incoming and normally reflected amplitudes are indicated by the blue vectors. The polarizer, aligned at a 45° angle relative to the plane of incidence in (a), is rotated by 90° in (b). Compare with Fig. 1 for a similar illustration of the conventional Kerr effects.

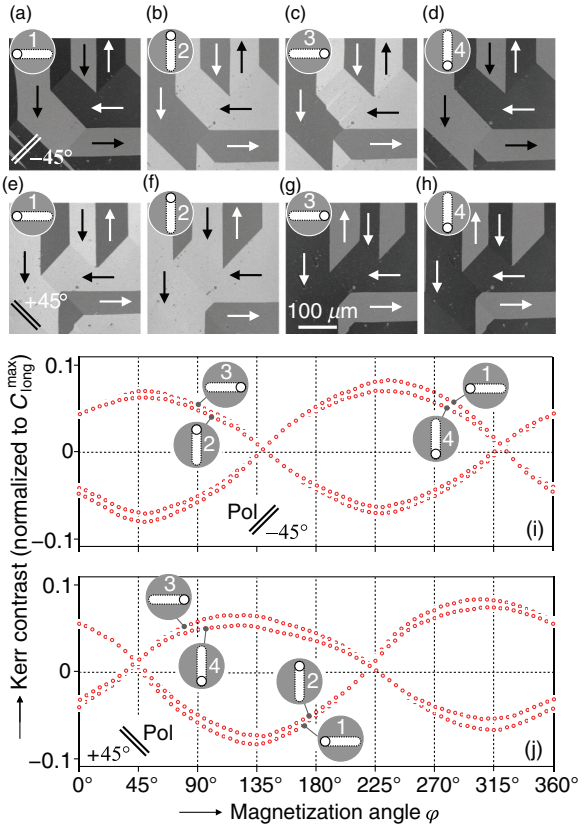

FIG. 7. Analyzer-free Kerr microscopy on the FeSi sheet by using red *linearly* polarized light at angles of ±45° relative to the planes of incidence. The domain images and the sensitivity curves were measured with all four LEDs, thus comprising all possibilities for the plane and direction of incidence. Domain images (a)–(d) were obtained at a polarizer setting of +45°, while the polarizer was at −45° for images (e)–(h). The contrast in (i) and (j) is again normalized to C_{max}^{long}.

the longitudinal 45°-dichroic reflection effects are of about equal strengths. The maximum contrast is ∼15% of C_{max}^{long}. Compared to the pure transverse contrast, it is thus reduced by a factor of approximately cos 45°, which is conceivable when considering the 45° rotation of the light compared to pure transverse conditions. The domain images in Fig. 7, obtained at polarizer settings of +45° [images in Figs. 7(a)–7(d)] and −45° [images in Figs. 7(e)–7(h)] confirm the phenomenology of the sensitivity curves. Both domains magnetized along as well as transverse to the plane of incidence show a comparable contrast as expected.

VII. LONGITUDINAL AND TRANSVERSE MCD-BASED KERR MICROSCOPY

In a recent article[18] mentioned in Sec. I, it was shown that the MO contrast of ultrathin magnetic films with perpendicular anisotropy can be significantly enhanced by embedding the magnetic media in between dielectric antireflection coatings, all deposited on a nonmagnetic mirror film. That work appears to be the first realization of a concept, which was suggested years ago:[48–50] By interference effects, the MO amplitude in an ultrathin magnetic film can be enhanced

while the regularly reflected light amplitude is reduced, leading to an increased MO rotation. (The ZnS antireflection layer, applied to the FeSi sample in our paper, has a similar effect on bulk metallic specimens.[42]) Although the authors in Ref. 18 talk about MOKE microscopy, the domains were actually imaged by *Faraday* microscopy, as the magnetic films are optically transparent and the light passes the films twice due to the mirror on the backside, thus resembling Faraday microscopy in reflection geometry. The improved Faraday signal made it also possible to realize analyzer-free MO microscopy by using *circularly polarized light* for illumination rather than plane-polarized light. By comparing Figs. 2(a) and 2(c), it is evident that a Kerr or Faraday rotation due to birefringence is not possible for circular illumination of a certain helicity; as for rotational effects, both left- and right-handed circular polarization is required. In circular light, however, only the magnetic dichroism effect can be active, as illustrated in Fig. 2(c). It leads to differently damped amplitudes for different magnetization directions that may result in a domain contrast. In a wide-field Kerr (or Faraday) microscope, a domain contrast should thus be generated, even in the absence of an analyzer [like for the pure transverse Kerr effect (Sec. V)]. In Ref. 18, this possibility of analyzer-free imaging was obviously demonstrated for the first time.

Encouraged by that work, we have replaced the linear polarizer with a circular polarizer, removed the analyzer, and dimmed the light in our wide-field Kerr microscope. As a sample, we again chose the in-plane magnetized FeSi sheet with antireflection coating[51] that was already studied by transverse Kerr microscopy (Sec. V). As being a nontransparent, bulk specimen, such a sheet can only be imaged in pure *Kerr* (i.e., reflection) geometry. Using circularly polarized light for illumination, a magnetic contrast for in-plane magnetization is expected to be achieved in both the transverse Kerr configuration [see Eq. (4)] and the longitudinal configuration [Eq. (5)].

In fact, it turned out that a domain contrast can readily be seen after background subtraction. Two series of images are presented in Fig. 8. The upper row was obtained with left-circular light and the lower row with right-circular light. Several observations are noteworthy:

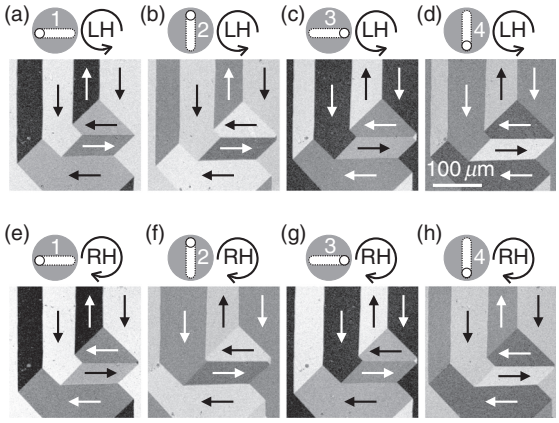

FIG. 8. Analyzer-free domain imaging on the FeSi material by using red *circular light* for illumination. The 635-nm quarter-wave plate was applied to generate the circularly polarized light. (a)–(d) Left-handed polarization and (e)–(h) right-handed polarization with all four LEDs separately activated as indicated. Shown are difference images of similar domain states.

- The contrast is inverted when the direction of incidence is inverted [compare, e.g., the images in Figs. 8(a) and 8(c) or Figs. 8(b) and 8(d)].
- Inverting the helicity of the light can lead to both a contrast inversion [compare, e.g., the images in Figs. 8(d) and 8(h)] or no inversion [like in the images in Figs. 8(a) and 8(e)].
- In all images, a domain contrast is seen for 180° domains magnetized both vertically and horizontally, so there is always contrast along and transverse to the plane of incidence. This indicates the simultaneous presence of longitudinal and transverse Kerr sensitivity.
- Different levels of domain contrast are seen. Domains transverse to the plane of incidence always show a stronger contrast than those magnetized along the incidence plane.

From the fact that the contrast of the vertical domains does not change sign in Figs. 8(a) and 8(e), and also Figs. 8(c) and 8(g), we can conclude that in the transverse configuration, the intensity contrast stems only from the *p*-polarized component of the circular light; i.e., the handedness does not play a role. On the other hand, the contrast inversion of the vertical domains in Figs. 8(b) and 8(f), and also Figs. 8(d) and 8(h), is due to A_L^C. Reversing the helicity reverses the contrast signal, as expected according to Eq. (5).

The in-plane contrast symmetry under circular illumination is obviously different from that of the conventional, rotation-based longitudinal Kerr effect and the pure transverse Kerr effect. This difference can readily be seen by comparing the sensitivity curves, obtained

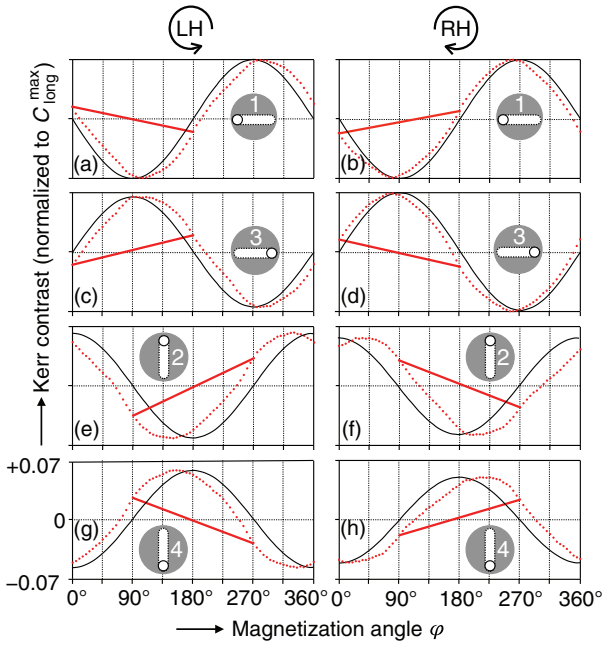

FIG. 9. Sensitivity curves for orthogonal planes of incidence, measured on the FeSi sheet by using left-handed [panels (a), (c), (e), and (g)] and right-handed ([panels (b), (d), (f), and (h)] circularly polarized, red light like in Fig. 8. A nonvanishing slope of the straight lines indicates the presence of longitudinal contrast contributions. Also plotted are $\pm\cos\varphi$ and $\pm\sin\varphi$ functions that are supposed to indicate pure transverse sensitivity curves for a visual comparison.

with circular light and displayed in Fig. 9, with those of the conventional longitudinal (Fig. 4) and pure transverse (Fig. 5) Kerr effects. At orthogonal planes of incidence, the latter is characterized by sin φ and cos φ functions that are in phase with intensity maxima and zero crossings at magnetization angles of (approximately) 0°, 90°, 180°, and 270°. In the case of circular polarization, the maxima and zero crossings are phase shifted compared to pure transverse sensitivity curves. In the left column of Fig. 9, this is shown for left-handed circular light, and in the right column, it is shown for right-handed circular light. To see the phase shift, the cosine and sine functions that would be expected under the (hypothetic) assumption of pure transverse sensitivities also have been added to the graph. Apparently, inverting the light helicity leads to an inversion of the phase shift direction. With light of the same helicity, the sensitivity curves are inverted for orthogonal planes of incidence [compare, e.g., the curves in Figs. 9(b) and 9(f) or in Figs. 9(d) and 9(h)].

The shapes of the sensitivity curves stem from the fact that with circular light, a combination of both A_T and A_L^C is measured simultaneously. For illustration, let us have a closer look at Fig. 9(e), which shows the sensitivity curve for LED-2 and left-handed light. For $\varphi = 90°$, $A_T = 0$, but $A_L^C \neq 0$. Near 45° both A_T and A_L^C are nonzero; their contributions can cancel each other depending on the values of Δ_{pp} and Δ_{sp} [in Fig. 9(e), cancelation occurs around $\varphi = 55°$]. At $\varphi = 0°$, A_T will be largest while $A_L^C = 0$. At $\varphi = 135°$, both A_T and A_L^C are again nonzero, but now A_L^C has a reversed sign, thus giving an additive enhancement of the contrast signal. Reversing the helicity [Fig. 9(f)] will reverse the A_L^C signal but not A_T. At the angles φ where the signals approximately canceled in Fig. 9(e), they will now enhance each other and *vice versa*.

According to Fig. 9, the curve shifts may vary between some degrees and 45°. This can be due to the "vectorial" mixing of signals in $|\vec{E}_{out}|^2$, which is not simply an addition, i.e., $B_L \cos\varphi \pm B_T \sin\varphi$, of two modulated amplitudes B_L and B_T. One can also see that the phase shifts are larger for LED-2 and -4. These are the two LEDs for which the light is reflected orthogonally at the beam splitter mirror [see Fig. 3(c)]. The beam splitter thus seems to have some influence on the light. We will address this again in Sec. VIII.

In any case, the essential finding is that circularly polarized light causes a dominating transverse Kerr sensitivity (i.e., sensitivity to magnetization components transverse to the plane of incidence) that is superimposed by a weaker longitudinal sensitivity (along the plane of incidence). In Fig. 9, we have drawn lines between the intensities at magnetization angles at which deviations from zero intensity are an indication for the existence of longitudinal contributions. The slopes of those curves immediately visualize the inversion of the longitudinal contrast on reversal of the helicity and direction of incidence. The overall maximum contrast, obtainable by using circularly polarized light, is ~15% of C_{max}^{long} and thus comparable to that of the longitudinal dichroic effect of Sec. VI.

VIII. POLAR MCD-BASED AND 45°-DICHROIC FARADAY MICROSCOPY

The existence of a polar, MCD-based Faraday domain contrast, caused by illumination with circular light, was already demonstrated in Refs. 18 and 22 as mentioned in Sec. I. In Fig. 10, a similar experiment is presented but now on the garnet film with perpendicular magnetization. In circular light [Figs. 10(b) and 10(c)], the domain contrast is reduced compared to the (conventional) Faraday contrast

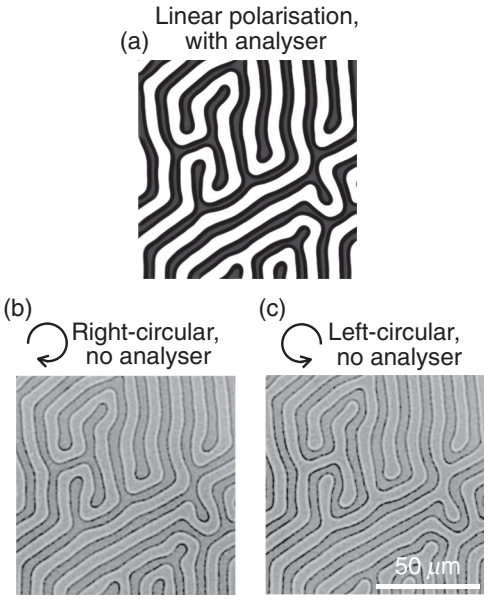

FIG. 10. Band domains in our garnet film magnetized perpendicular to the film plane and imaged at perpendicular incidence. (a) Conventional polar Faraday microscopy using plane-polarized light and an analyzer. In (b) and (c), right- and left-handed circularly polarized light was used without an analyzer. Red light was used, which in garnet material leads to slightly better contrast than white light (not shown). Like in Figs. 8 and 9, the 635-nm quarter-wave plate was applied to generate the circular light. All images are live images without background subtraction.

that is optimized with the analyzer [Fig. 10(a)]. Inverting the handedness of the circular light leads to an inversion of the domain contrast, as expected. It needs to be noted that the MCD-based domain contrast on this specific specimen significantly depends on the selected focal depth of the microscope. (A much stronger contrast than that visible in Figs. 10(b) and 10(c) can be obtained by defocusing the transparent garnet film by some micrometers [not shown].)

Interestingly, a domain contrast on the garnet film can also be seen by illumination with *plane-polarized* light and omitting the analyzer (Fig. 11). It has a curious symmetry, being maximal at polarizer settings of ±45° with inverted contrast. It thus resembles the phenomenology of the longitudinal dichroic Kerr contrast found on illuminating in-plane magnetized material with plane-polarized light (Sec. VI). It looks conceivable to address this contrast to the equivalent *polar dichroic effect* A_L^P, which was mentioned in Sec. II. There also is, however, a further effect that should lead to a domain contrast with the same phenomenology and that arises from the reflector module [Fig. 3(c)] in our regular wide-field microscope: At polarizer settings along the x and y axes, the light is mirrored toward the sample by keeping its polarization direction and linear character. Linearly polarized light, falling on a specimen with up- and down-magnetized domains along the propagation direction, will lead to circular birefringence and circular dichroism [see Figs. 2(a) and 2(b)]. Without an analyzer, however, the rotation due to birefringence cannot be detected, and the dichroism effect leads to nondetectable ellipticity anyway. Therefore, no domain contrast is seen in Figs. 11(a) and 11(c).

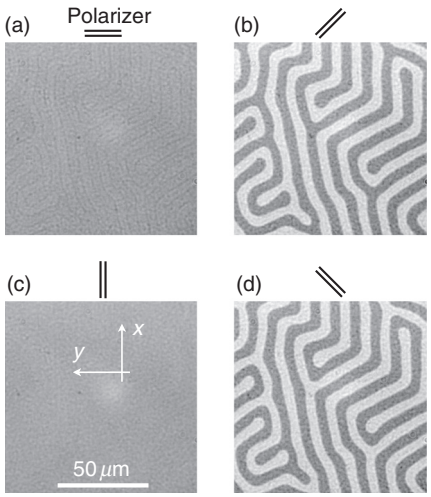

FIG. 11. Same garnet band domains as in Fig. 10, again imaged at perpendicular incidence but now in *plane-polarized* light at four settings of the polarizer as indicated. Like in Fig. 10, the analyzer was removed from the microscope. The domain boundary contrast in (a) and (somewhat weaker) in (c), which shows up at horizontal and vertical polarizer settings, will be discussed in detail in Sec. XII C. At polarizer settings of ±45° in (b) and (d), the domains appear in regular, areal contrast that is inverted when the polarizer is rotated by 90° [compare (b) and (d)].

If the polarization plane deviates from the x and y axes, however, the x and y components of the light are mirrored with a phase shift, leading to elliptically polarized light. Ellipticity will be maximal at the polarizer angle of 45°, and it will be inverted at −45°. The elliptical waves can well induce a circular (better "elliptical") dichroism effect, thus resulting in a domain contrast that is strongest at polarizer settings of ±45° and that disappears at 0° and 90°, in agreement with Fig. 11. Experimentally, it is difficult to uniquely assign the 45° contrast to one of the two effects.

Although a domain contrast is not seen at polarizer settings of 0° and 90° [Figs. 11(a) and 11(c)], the domain boundaries nevertheless show up with a dark line contrast, as can be seen by a closer inspection of the two images. In Fig. 11(a) the line contrast is directly visible, while in Fig. 11(c) it only shows up after background subtraction (not shown). This domain boundary contrast is caused by magneto-optical diffraction. Let us postpone the discussion of such effects to Sec. XII C.

IX. POLAR MCD-BASED AND 45°-DICHROIC KERR MICROSCOPY

Finally, we have tested the encouraging results of polar MCD-based Faraday microscopy (Sec. VIII) also on an ultrathin CoFeB metallic film with perpendicular anisotropy. Different from the mentioned experiments in Ref. 18, no mirror film was deposited underneath the magnetic film in our case so that it is justified to talk about true "MOKE" microscopy. Furthermore, we did not surround the magnetic film by interference layers. While by conventional polar Kerr microscopy a domain contrast can readily be seen without image processing [Fig. 12(a)] that can be infinitely enhanced by background subtraction [Fig. 12(b)], a contrast is hardly visible in analyzer-free Kerr

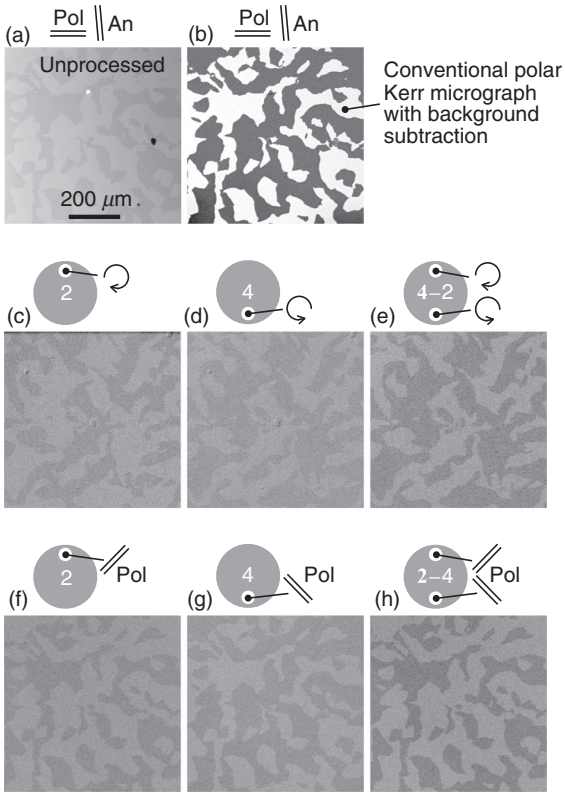

FIG. 12. Domains in Ta(3)/**CoFeB(0.9)**/MgO(1)/Ta(3) (thickness in nm) film with perpendicular anisotropy, imaged by Kerr microscopy under different conditions. (a) By conventional polar Kerr microscopy at perpendicular incidence. (b) Background subtraction significantly enhances the contrast. (c), (d), and (e) Analyzer-free imaging in circular (better elliptical) light and (f), (g), and (h) by using plane-polarized light at oblique incidence (see the text for details). White light was used for illumination, and for circular polarization, the 550-nm quarter-wave plate was applied.

microscopy in an unprocessed image (not shown). After background subtraction, however, domains are well seen by using circular polarization [Fig. 12(c)] as well as plane-polarized light [Fig. 12(f)]. For the latter, the polarizer has to be set at ±45° as elaborated in Fig. 11. In both cases, the strength of the contrast after background subtraction is comparable to that of an unprocessed image in the conventional polar Kerr mode [compare the images in Figs. 12(c) and 12(f) with the image in Fig. 12(a)].

This contrast can be further enhanced by activating two LEDs at opposite locations, running them in the pulsed mode, and subtracting the two corresponding images with proper normalization—a concept that was introduced in Ref. 39 for the enhancement of contrast in conventional longitudinal Kerr microscopy. In Fig. 10, we see that the polar dichroic Faraday contrast is inverted by using LCP and RCP light. The same is true for the polar dichroic Kerr contrast as demonstrated in Figs. 12(c) and 12(d). This is the polar equivalent of the longitudinal MCD in reflection [Eq. (5)]. Here, we have placed two linear polarizers with polarization axes along the x and y axes in the aperture plane of the microscope (which is confocal to the back focal plane of the objective lens), one in the illumination path of LED-2 and the

other in the path of LED-4, and both followed by a quarter-wave plate that is oriented at 45°. Consequently, the light of LED-2 and LED-4 is right- and left-circularly polarized, respectively. Note that now we have an oblique incidence of light at an angle of ∼25°, which, however, has no significant influence on the polar Kerr effect that scales with the cosine of the angle of incidence. By running the two LEDs in the pulsed mode in synchronization with the camera and by subtracting the two obtained images with inverted contrast, the contrast in the difference image is actually doubled after proper normalization [see Fig. 12(e)].

The same concept can also be applied to analyzer-free imaging in plane-polarized light [Figs. 12(f) and 12(g)]. Here, the light of the two LEDs was linearly polarized at ±45°, in accordance with the polar dichroic reflection effect mentioned in Sec. II. The magnetic contrast is proportional to $Q_V \sin 2\theta$, with θ the angle of the plane polarization with respect to the reflection plane. This gives a maximum contrast for $\theta = 45°$ and an inverted contrast for 135°, as seen in Figs. 12(f) and 12(g). Taking the difference image thus doubles here as well the contrast [cf. Eq. (6)]. As previously mentioned when discussing the garnet film in Sec. VIII, the mechanism of the contrast formation needs to be scrutinized further. Notwithstanding, the pulsed mode makes analyzer-free, intensity-based Kerr microscopy applicable also to ultrathin magnetic films without the necessity of dielectric interference layers.

Those pulsed modes for contrast enhancement rely on the subtraction of two images with inverted contrast obtained by choosing oppositely arranged LEDs for illumination. Consequently, they are only possible for oblique incidence of light. An interesting alternative for the case of circular polarization, which should also work for perpendicular incidence, might be worth examining: In Ref. 52, methods for (general) dichroism microscopy were suggested, which allow for a periodic and discrete alternation of the incident polarization between left- and right-circularly polarized light by using a photoelastic modulator or a beam displayer combined with a chopper and quarter-wave plate in the illumination path. Synchronizing the alternating polarization with the camera exposure and subtracting the corresponding two images should lead to the same kind of contrast enhancement as shown in Fig. 10.

X. MLD-BASED VOIGT AND GRADIENT MICROSCOPY

As introduced at the end of Sec. II, the main difference of the Voigt contrast compared to the Kerr (or Faraday) contrasts is its quadratic dependence on the magnetization direction. In conventional analyzer- and compensator-based Voigt microscopy, an in-plane magnetized specimen is illuminated at perpendicular incidence, thus suppressing the Kerr (or Faraday) effect. In the case of an Fe(100) surface, the polarization plane needs to be at 45° to the two easy axes to obtain maximum Voigt domain contrast.[7]

The experimental conditions are different when the MLD effect is applied directly in an analyzer-free microscope. This is demonstrated in Fig. 13 for our FeSi sample. Perpendicular incidence of (red) light was chosen to avoid any of the other contrast phenomena discussed so far, and the polarizer was rotated in steps of 45°. Maximum domain contrast is found when the light is polarized along the two anisotropy axes, and this contrast is inverted by rotating the polarizer by 90° [compare Figs. 13(a) and 13(b)]. This phenomenology clearly demonstrates that the different absorption of the two linearly polarized

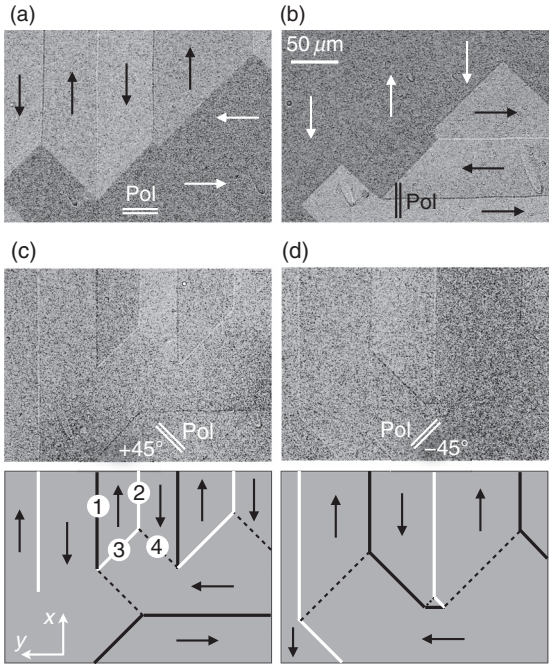

FIG. 13. Domains on the FeSi sheet imaged in red light at perpendicular incidence. The polarizer was set along the x and y axes and at angles of ±45° as indicated. The contrast in (a) and (b) is due to the reflection MLD effect and the gradient effect, while (almost) pure gradient contrast is seen in (c) and (d). The schematics in (c) and (d) trace the gradient contrast of the corresponding domain images.

partial waves due to the MLD effect (see Sec. II) is responsible for the observed contrast. In our case, domains magnetized along the polarization axis obviously lead to a stronger absorption and, thus, a darker color compared to those magnetized transverse to the polarization axis. At polarizer settings of ±45° [Figs. 13(c) and 13(d)], the domain contrast disappears, as now the two orthogonal easy axes absorb the light equally.

It should be noticed that the quadratic effect, measured in Figs. 5(d) and 5(e) by illumination of the same sample with *s*-polarized light at *oblique* incidence is as well caused by the MLD effect. Under those conditions, the transverse Kerr effect is not possible, and the longitudinal Kerr effect, being well possible though, leads to a light rotation that cannot be detected without an analyzer. The basic conditions with the polarizer along one of the two easy axes are, however, suitable for the MLD effect. Also, the phase of the quadratic function in Fig. 5(e) corresponds to expectations; the contrast is maximal at magnetization angles along the easy axes rather than along the diagonal direction, which would be true in analyzer-based Voigt microscopy.

The domain boundary contrasts, visible in all images of Fig. 13, are caused by the MO gradient effect.[7,36,53] As mentioned in Sec. I, the gradient effect is sensitive to gradients in the magnetization vector field, which are strongest across domain walls. Already in the original work when this effect was discovered,[36] it was noticed that the effect occurs under the same experimental conditions as the Voigt effect and that it can be described phenomenologically by the dielectric law[36,54]

$$\vec{D} = P_{\mathrm{gr}} \begin{pmatrix} -\frac{\partial m_x}{\partial y} - \frac{\partial m_y}{\partial x} & \frac{\partial m_x}{\partial x} - \frac{\partial m_y}{\partial y} \\ \frac{\partial m_x}{\partial x} - \frac{\partial m_y}{\partial y} & \frac{\partial m_x}{\partial y} + \frac{\partial m_y}{\partial x} \end{pmatrix} \vec{E}_{\mathrm{in}}, \tag{7}$$

in which the tensor contains various gradients of the in-plane magnetization components. The material constant P_{gr} scales with that of the Kerr effect (Q_{V}). Like for (conventional) Voigt microscopy, for gradient microscopy, a compensator and analyzer were needed for contrast adjustment, with the latter being aligned perpendicular to the polarizer. The effect was therefore described by just considering the off-diagonal elements of the dielectric tensor; an incoming wave, polarized along the x direction for instance, will induce a MO component along the y axis according to $D_y = \epsilon_{yx} E_{\mathrm{in},x}$ that is detected by the crossed analyzer along the y axis. At that time,[36] the diagonal elements of the tensor (ϵ_{xx} and ϵ_{yy}) were only added for symmetry reasons, pointing out that those components would just lead to an amplitude modulation of the reflected light that cannot be detected with the analyzer.

Without an analyzer, however, it is exactly those diagonal terms containing mixed derivatives that are responsible for the gradient contrast symmetry in the images of Fig. 13. For a more detailed discussion, we need to consider the magnetic microstructure of domain boundaries, an aspect that was discovered by Kamberský.[55,56] In Eq. (7), each tensor component contains sums of gradients rather than single gradients. Such sum terms are necessary for specimens in which subsurface, perpendicular gradients are relevant to fulfill the condition $\mathrm{div}\,\vec{m} = 0$, which is, e.g., the case for so-called V-lines in an iron-like material.[3] In our case, we can neglect subsurface gradient components if we assume that the light—within the information depth—does not interact with the internal Bloch component of the stray-field free vortex domain walls.[3] A strict in-plane magnetization can then be assumed, the wall magnetization itself can be neglected, and only the magnetization gradients across the domain walls are relevant. The dielectric tensor is then simplified and we get

$$\vec{D} = P_{\mathrm{gr}} \begin{pmatrix} -\frac{\partial m_y}{\partial x} & \frac{\partial m_x}{\partial x} \\ -\frac{\partial m_y}{\partial y} & \frac{\partial m_x}{\partial y} \end{pmatrix} \vec{E}_{\mathrm{in}}. \tag{8}$$

This dielectric expression can now be applied to verify the domain boundary contrast in Fig. 13. Let us take the marked walls in Fig. 13(c) as an example. Here, the light is polarized at +45°, so the x and y components of the electrical field vector $\vec{E}_{\mathrm{in}}$ are equal. For domain wall 1, only the gradient $\frac{\partial m_x}{\partial y}$ is nonzero and negative. It thus causes a negative D_y component that opposes the normally reflected E_y component, leading to an amplitude decrease and, consequently, a dark domain boundary contrast. For domain wall 2, it is opposite; here again only the gradient $\frac{\partial m_x}{\partial y}$ is nonzero but now positive. It thus leads to an increase in the E_y component and a white boundary contrast. For wall 3, we get $\frac{\partial m_x}{\partial x}, \frac{\partial m_x}{\partial y} > 0$ and $\frac{\partial m_y}{\partial y}, \frac{\partial m_y}{\partial x} < 0$. Consequently, all components of the dielectric tensor become positive so that both components of the reflected electrical field vector experience an amplitude increase, leading to a white boundary contrast. In the case of wall 4, it is opposite. Here, we find $\frac{\partial m_x}{\partial x}, \frac{\partial m_y}{\partial x} < 0$ and $\frac{\partial m_y}{\partial y}, \frac{\partial m_x}{\partial y} > 0$. The four components of the tensor, therefore, change sign alternately so that neither component of the $\vec{D}$ vector adds to the normally reflected field vector. This domain wall will therefore not show up with a contrast. Based on Eq. (8), the observed contrasts of all domain boundaries in Fig. 13 can be verified.

XI. KERR MICROSCOPY WITH SEPARATED PATHS

To check for eventualities, we have tried to verify our findings by looking for the same effects and contrasts in our microscope with separated illumination and reflection paths [Fig. 3(d)], again by omitting the analyzer. The results are summarized in Fig. 14:

- The sensitivity curves for pure transverse Kerr microscopy could be verified [compare Figs. 5(e) and 14(a)]. Also, the domain contrast confirms pure transverse sensitivity [compare Figs. 5(a) and 5(b) and Fig. 14(g)].
- The quadratic MLD contrast, found for the oblique incidence of *s*-polarized light, could be verified [compare Figs. 5(e) and 14(b)].
- The longitudinal dichroic contrast, observed for plane-polarized light at an angle of 45° relative to the plane of incidence, could

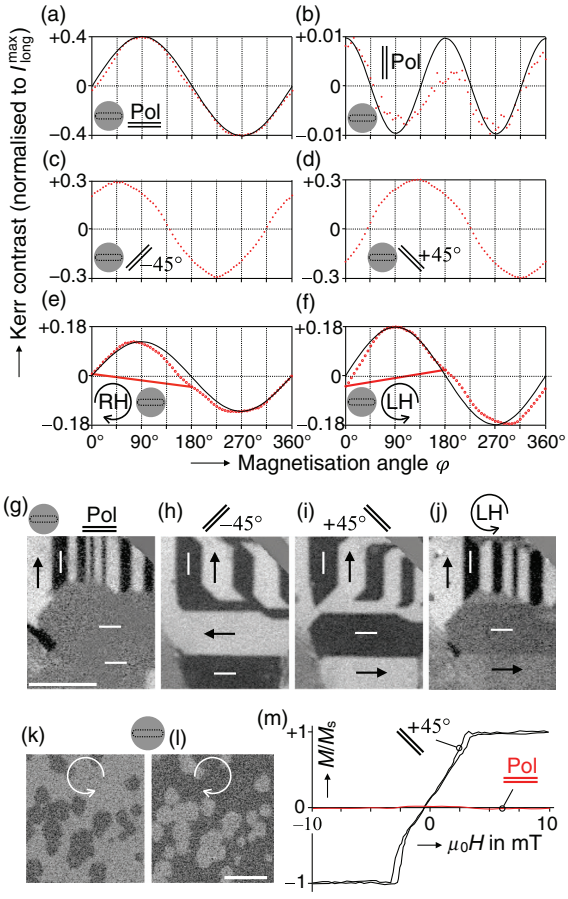

FIG. 14. Measurements and low-resolution domain observations in the microscope with separated illumination and reflection paths. (a)–(f) Sensitivity curves on the FeSi specimen measured in red light under the indicated conditions. (g)–(j) Exemplary domain images, revealing the characteristic contrast features that are expected from the curves. (k) and (l) Nucleated domains in the Pt/Co/Pt film with perpendicular anisotropy, observed in white, circularly (better elliptically) polarized light of opposite helicities. (m) Hysteresis curves of the garnet film in perpendicular field measured with red, plane-polarized light at the indicated polarizer settings. For circular polarization, the 550-nm quarter-wave plate was applied.

also be verified [compare the images and curves in Fig. 7 with the curves in Figs. 14(c) and 14(d) and the images in Figs. 14(h) and 14(i)]. The presumed elliptical light contribution, generated by the beam splitter in our regular microscope, does not seem to have a significant influence for this effect.

- The phase shift symmetry by using circularly polarized light, indicating the presence of transverse sensitivity with superimposed (weaker) longitudinal sensitivity, could be verified [compare the curves in Fig. 9 with Figs. 14(e) and 14(f) and the domain images in Fig. 8 with Fig. 14(j)].
- On perpendicularly magnetized films, we could verify the presence and symmetry of the MCD-based Kerr contrast [Figs. 14(k) and 14(l)].
- The existence of a *polar* dichroic contrast, expected for plane-polarized light at an angle of ±45° relative to the incidence plane, could be verified on the garnet film, i.e., in Faraday geometry. As the domain width is below resolution, we have measured the hysteresis curve on this specimen in a magnetic field perpendicular to the film plane for demonstration [Fig. 14(m)]. For a polarizer setting of 0°, no MO signal was found, as expected. However, we did not find any polar contrast for metallic films with perpendicular anisotropy, i.e., for Kerr geometry. The contrasts in Figs. 12(f) and 12(g) could thus not be reproduced. This indicates, as explained in Sec. VIII, that in this case, the generation of elliptically polarized light due to the mirror in the beam splitter must be responsible for the contrasts in Fig. 12 and not the 45°-dichroic contrast. It seems that the polar 45°-dichroic *Kerr* contrast is not strong enough to be detected in contrast to the polar dichroic *Faraday* contrast.

XII. FURTHER ASPECTS

Let us finally point out three further findings related to the previously described phenomena without going into much detail, i.e., leaving them open for future examinations.

A. Influence of light color

In Fig. 15, we have collected some representative sensitivity curves that were obtained on the FeSi sample at the indicated conditions. The curves were measured with blue, red, and white light, and the intensities are normalized to the maximum intensity in each case. Therefore, the fact that the absolute amplitude of the Kerr signal depends on the wavelength, as mentioned several times throughout the paper, is not visible in the graphs. It becomes obvious, however, that (besides the signal amplitude) the phase of the measured curve also can be more or less color dependent. We furthermore point out that for the experiments in Fig. 15, a quarter wave plate was used to generate circularly polarized light that is not optimized to either of the three colors. In each case, the light will therefore be more elliptically polarized rather than strictly circular. It is thus expected that the MCD signals can be enhanced by using monochromatic light with a wavelength that is adapted to the Kerr spectra of the material under investigation together with wavelength-specific circular polarizers.

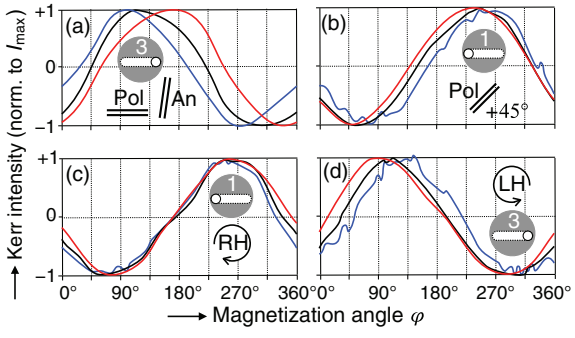

FIG. 15. Selected sensitivity curves measured on the FeSi sample under the indicated conditions by using red, blue, and white light. The maximum intensities have been equalized for all curves to emphasize the phase of the curves. In absolute numbers, the contrasts in (a) are ∼40% of C_{max}^{long} for white and blue light. In (b)–(d), they are ∼12% for red light and ∼7% for blue and white light. For circular polarization, the 550-nm quarter-wave plate was applied.

B. Imaging without analyzer and polarizer

Figure 16 demonstrates that domains in FeSi can even be seen without any polarizer in the normal wide-field polarization microscope. A closer inspection of the domain contrast reveals that the transverse Kerr effect dominates, which is understandable as this effect should exist even for unpolarized light. Nonetheless, a domain contrast was also seen on the perpendicularly magnetized garnet and Co/Pt/Co films in a (our) normal wide-field microscope (not shown). The transverse contrast on the FeSi specimen could be verified in the microscope with separated paths [Fig. 3(d)] after also omitting the polarizer, thus confirming that the transverse Kerr effect does not require plane-polarized light. However, in the microscope with separated paths, no indication of domain contrast could be seen on the films with perpendicular anisotropy. The occurrence of polar contrast in our normal microscope may thus be attributed to the beam splitter [Fig. 3(c)], which seems to be responsible for a net elliptical component of the incident light that causes an MCD-based polar Kerr effect. Furthermore, it cannot be excluded that the lenses in the microscope along the illumination path also can generate elliptically polarized light, possibly caused by mechanical stress in the glasses.

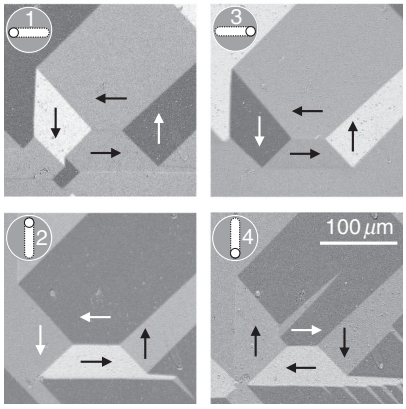

FIG. 16. Domain images on the FeSi sheet observed by using red light in the normal Kerr microscope but *without an analyzer and polarizer*. Shown are four images of similar domain states that were obtained with four directions of incidence as indicated. The dependence of the contrast on the plane of incidence clearly indicates a dominance of the transverse Kerr effect.

C. Diffraction effects

In Fig. 11(a), we have seen that the domain walls in our garnet film show up as a dark line contrast when imaged at a polarizer setting of 0° in the absence of the analyzer. In Fig. 17(a), this contrast is shown again on a similar domain pattern, but now enhanced by background subtraction. By such enhancement, a black (though lower) line contrast is also seen for a polarizer setting of 90° (not shown). The line contrast cannot be caused by the wall magnetization itself as the Bloch wall width in such garnet films is in the 10-nm range, which is well below the resolution of 640 nm for the given objective lens and wavelength. Also, the magneto-optical gradient effect cannot be responsible for this boundary contrast as any gradient contrast should change sign at every other wall.

Black domain boundary contrasts have already been observed by regular, rotation-based magneto-optical microscopy on in-plane magnetized iron films in the early 1960s[57] (see Ref. 58 for a review). In Figs. 17(b)–17(d), the principle is documented for our garnet film by applying conventional, analyzer-based Faraday imaging using plane-polarized light. As expected, the domain contrast is inverted by inverting the analyzer opening direction [compare Figs. 11(b) and 11(c)]. This is due to polar Kerr vectors of opposite signs that are generated by the antiparallel domains and which are pointing perpendicular to the polarizer axis, thus causing clockwise and counterclockwise rotations of the emerging wave (see Fig. 1). If the analyzer is crossed to the polarizer [Fig. 17(d)], the two Kerr amplitudes transmitted by the analyzer have the same magnitude, and the two domain phases will consequently reflect the light with equal intensities, thus not causing any domain contrast. However, the two opposite Kerr amplitudes are phase shifted by 180°. Therefore, they interfere destructively within a region around the walls that is determined by the lateral resolution, leading to dark lines at the domain boundaries. As the line contrast is caused by phase shifts, it may be classified as *phase contrast*.[58] Note that this phase contrast does not depend on the wall magnetization itself as long as the wall width is below resolution. The same is true for the gradient effect;[36] in both cases, only the domain magnetization on both sides of the domain walls is responsible for the domain boundary contrasts. If the analyzer would be set parallel to the polarizer, the Kerr amplitudes would be blocked so that the light would not experience any magnetization-dependent amplitude or phase changes by passing the specimen.

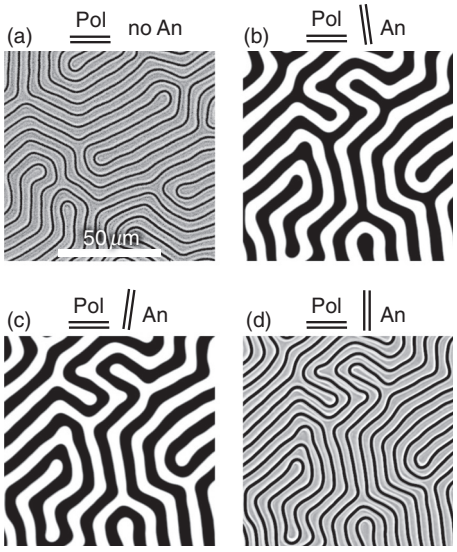

FIG. 17. Magneto-optical phase and domain contrast imaged on the garnet film in plane-polarized, red light at perpendicular incidence. (a) Phase contrast without an analyzer, (b) and (c) conventional domain contrast with an oppositely opened analyzer, and (d) phase contrast with crossed analyzer and polarizer. Images (a) and (d) are difference images for which a background image was subtracted to enhance the contrasts. For the "nonmagnetic" background image, an AC magnetic saturation field perpendicular to the film plane was applied, and the resulting oscillating image intensity was averaged.

The domain boundary contrast in Fig. 17(a) can be interpreted along the same line. We have seen that the prerequisites for phase contrast at domain boundaries is the presence of phase-shifted Kerr (or Faraday) amplitudes and the absence of domain contrast. The latter was achieved by the crossed analyzer in the case of Fig. 17(d). In the geometry of Fig. 17(a), the Faraday amplitudes are the same as in the previous case, and the absence of domain contrast is intrinsically given. The domain boundary contrast in Fig. 17(a) may consequently be interpreted as *phase contrast*.

It should also be noted that the phase contrast depends on the illumination aperture.[58] Fresnel diffraction fringes may show up for small apertures, while other contrast artifacts may be superimposed in the case of oblique light incidence. In Ref. 36, it was shown that a kind of schlieren effect may occur if perpendicularly magnetized domains are observed at oblique incidence with small aperture and if the reflected beam passes close to an edge of the aperture. The mentioned phase jump then leads to differently deflected beams at neighboring domain walls, which are either cut off by the aperture or deflected into the aperture, thus resulting in an alternating bright and dark appearance of neighboring domain boundaries that may be superimposed on the polar gradient effect. Prerequisite is again the suppression of domain contrast, e.g., by crossed polarizer and analyzer.

Talking about diffraction effects at domain boundaries, let us finally mention *dark-field microscopy*. In the previous discussions, we have seen that the light, passing a domain structure, consists of a normal amplitude and a magnetization-dependent Kerr or Faraday amplitude that is polarized perpendicular to the incoming, plane-polarized wave. As the normal amplitude does not contain magnetic information, it needs to be suppressed or at least reduced. In conventional, bright-field Kerr and Faraday microscopy, this is achieved by an (almost) crossed analyzer. The presence of a magneto-optical amplitude, however, is independent of the presence or absence of an analyzer. Those components will as well be present if the normal component is suppressed by running an optical polarization microscope in the dark-field mode. In Refs. 53, 58, and 59 it was shown that in the dark-field microscopy the domain boundaries show up as *bright lines*, even in the absence of any polarizing element. Adding a polarizer and analyzer may help to separate those magnetic line contrasts from the superimposed contrast emerging from nonmagnetic, topographic features, like scratches that show up under the same conditions. In Fig. 18, the dark-field contrast was reproduced for our garnet film without using any polarizing element.

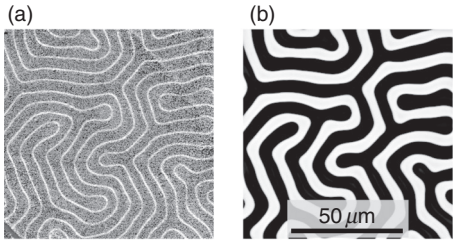

FIG. 18. (a) Dark-field image of the garnet film observed in white light by means of a Carl Zeiss dark-field reflector and a 20× HD DIC objective without polarizer and analyzer. Shown is a difference image to enhance the contrast. (b) Corresponding regular Faraday image obtained in red light by means of the analyzer.

XIII. CONCLUSIONS

Different from conventional magneto-optical Kerr and Faraday microscopy, we have demonstrated that it is also possible to image magnetic domains in an optical wide-field polarization microscope without needing an analyzer. We have shown that using plane-polarized light for illumination, the transverse Kerr effect can be employed on in-plane magnetized materials when the light has a *p*-component and the magnetization has a component perpendicular to the incidence plane being maximum for $\vec{k} \perp \vec{m}$ with $\vec{k}$ as the wave vector. Furthermore, we have shown that the transverse Kerr effect is even active in the absence of the polarizer, thus not requiring plane-polarized light at all. In circularly or elliptically polarized light, materials with in- and out-of-plane magnetization can be imaged when $(\vec{k} \cdot \vec{m}) \neq 0$. Here, the domain contrast is caused by magnetization-dependent intensity modulations due to the MCD. This works in both transmission (Faraday) and reflection (Kerr) geometry. A further magnetic intensity contrast can be obtained for longitudinal in-plane magnetizations, using plane-polarized light at a nonzero angle θ ($\approx \pm 45°$) with respect to the incidence plane, also when $(\vec{k} \cdot \vec{m}) \neq 0$. The MLD, finally, provides a weaker contrast mechanism than the MCD, but it could be applied for situations where the MCD is not effective, for example, the visualization of antiferromagnetic domains.

While our study draws attention to intensity modulation effects for imaging, it deserves to be noted that even in conventional Kerr microscopy, one needs to consider that such effects may be superimposed onto the conventional contrasts. This is most obvious for the transverse Kerr effect, which may lead to phase-shifted sensitivity curves in the case of the longitudinal Kerr microscopy with *s*-polarized light as demonstrated in Fig. 4. But also, the curve distortions, visible in that figure, may be related to superimposed quadratic effects or MCD effects being caused by elliptical light contributions due to the beam splitter or stressed optical components in the microscope. Furthermore, the phase contrast at domain boundaries (Fig. 17) may be superimposed to conventional domain images at insufficient analyzer opening angles.

While the MCD effect, induced by magnetic fields at visible light frequencies, plays an established role in the investigation of molecular electronic structure and transitions by using spectroscopic methods,[9] its potential for magnetic imaging has apparently been disregarded so far. MCD microscopy with visible light thus provides an interesting alternative to the more elaborate techniques that are based on XMCD.[24,25] Provided that the amplitude modulations are large enough, analyzer-free wide-field MO microscopy would also offer some advantages compared to conventional and analyzer- and compensator-based microscopy. (i) The analyzer and the compensator, necessary for contrast optimization in a conventional MO microscope, can be omitted, thus reducing the number of optical elements and with it the complexity of contrast adjustment. (ii) In conventional MO microscopy, one usually works at almost crossed polarizer and analyzer, i.e., the overall image intensity is rather low, requiring light sources with a high luminous density, polarizers with high transmittance, and advanced cameras with high sensitivities to achieve domain images with good signal-to-noise ratios. In analyzer-free MO microscopy, the requirements for light source, polarizers and cameras are much more relaxed as the image brightness posses no problem. (iii) The maximum domain contrasts in the analyzer-free modes are reduced by a factor of ∼10 compared to the best contrasts obtained by conventional longitudinal and polar Kerr microscopy. Using monochromatic light and wavelength-specific circular polarizers helps to improve the signal in the case of the MCD effect. For quantitative Kerr microscopy, which relies on well-defined sensitivity curves to calibrate the domain contrast, the pure transverse Kerr effect (see Fig. 5) seems to be the best choice. Overall, we find that enhanced by background subtraction, the achievable contrast for both in-plane and perpendicularly magnetized media does not suffer significantly compared to conventional domain contrasts.

To summarize, our study highlights possible approaches for performing magnetic domain imaging in intensity-based, wide-field magneto-optical microscopy. Implementing these approaches can make magnetic domain imaging widely available in simplified microscopy setups.

ACKNOWLEDGMENTS

R.S. acknowledges stimulating discussions with Vladislav Demidov (Universität Münster). I.S. is grateful to the Deutsche Forschungsgemeinschaft (German Research Foundation) for supporting this work (Project No. SO 1623/2–1), and P.M.O. acknowledges support from the Swedish Research Council (Vetenskapsrådet, Project No. 2017-04481). A.V.O. thanks the Russian Foundation for Basic Research (Grant No. 19-02-00530) and Deutscher Akademischer Austauschdienst (DAAD, Grant No. 57447934). A.S.S. acknowledges the support of the Russian Ministry of Science and Higher Education for state support of scientific research conducted under the supervision of leading scientists in Russian institutions of higher education, scientific foundations, and state research centers (Grant No. 075-15-2021-607) and Act 211 of the Government of the Russian Federation (02.A03.21.0011). The sample preparation and experimental studies were partially supported by the Russian Science Foundation (Grant No. 19-72-20071). We thank Professor Young Keun Kim (Korea University, Seoul, South Korea) and his group for providing the Ta/CoFeB/MgO/Ta film. Technical support by Stefan Pofahl (IFW) is acknowledged. Special thanks to Heiner Eschrich and Michael Zölffel (Carl Zeiss AG, Jena, Germany) for valuable advice on optical microscopy. The authors thank Michal Urbánek (Brno, Czech Republic) for providing the Pt/Co/Pt film.

DATA AVAILABILITY

The data that support the findings of this study are available from the corresponding author upon reasonable request.

REFERENCES

[1]S. Bader, "Smoke," J. Magn. Magn. Mater. **100**, 440–454 (1991).
[2]"Wide-field" optical microscopy is the conventional microscopy technique in which the whole area of interest is exposed to light and then simultaneously viewed either by eye or a camera. This is different from optical scanning microscopy, a sequential imaging technique in which a spot of light is scanned relative to the specimen in a raster-like way, building up an image point by point.
[3]A. Hubert and R. Schäfer, *Magnetic Domains: The Analysis of Magnetic Microstructures* (Springer-Verlag, 1998).
[4]R. Schäfer, "Investigation of domains and dynamics of domain walls by the magneto-optical Kerr-effect," in *Handbook of Magnetism and Advanced Magnetic Materials* (John Wiley & Sons, 2007).
[5]J. McCord, "Progress in magnetic domain observation by advanced magneto-optical microscopy," J. Phys. D Appl. Phys. **48**, 333001 (2015).
[6]S. Egelkamp and L. Reimer, "Imaging of magnetic domains by the Kerr effect using a scanning optical microscope," Meas. Sci. Technol. **1**, 79–83 (1990).
[7]W. Kuch, R. Schäfer, P. Fischer, and F. Hillebrecht, *Magnetic Microscopy of Layered Structures* (Springer-Verlag, 2015).
[8]P. M. Oppeneer, "Magneto-optical Kerr spectra," in *Handbook of Magnetic Materials*, Vol. 13, edited by K. H. J. Buschow (Elsevier, 2001), pp. 229–422.
[9]W. R. Mason, *A Practical Guide to Magnetic Circular Dichroism Spectroscopy* (Wiley-Interscience, 2007).
[10]P. Fischer, G. Schütz, G. Schmahl, P. Guttmann, and D. Raasch, "Imaging of magnetic domains with the x-ray microscope at BESSY using x-ray magnetic circular dichroism," Z. Phys. B Cond. Matter **101**, 313 (1997).
[11]J. Stöhr, H. A. Padmore, S. Anders, T. Stammler, and M. R. Scheinfein, "Principles of x-ray magnetic dichroism spectromicroscopy," Surf. Rev. Lett. **5**, 1297–1308 (1998).
[12]C. M. Schneider and G. Schönhense, "Investigating surface magnetism by means of photoexcitation electron emission microscopy," Rep. Prog. Phys. **65**, 1785–1839 (2002).
[13]F. Nolting, A. Scholl, J. Stöhr, J. W. Seo, J. Fompeyrine, H. Siegwart, J.-P. Locquet, S. Anders, J. Lüning, E. E. Fullerton, M. F. Toney, M. R. Scheinfein, and H. A. Padmore, "Direct observation of the alignment of ferromagnetic spins by antiferromagnetic spins," Nature **405**, 767–769 (2000).
[14]A. Scholl, J. Stöhr, J. Lüning, J. W. Seo, J. Fompeyrine, H. Siegwart, J.-P. Locquet, F. Nolting, S. Anders, E. E. Fullerton, M. R. Scheinfein, and H. A. Padmore, "Observation of antiferromagnetic domains in epitaxial thin films," Science **287**, 1014–1016 (2000).
[15]H.-C. Mertins, D. Abramsohn, A. Gaupp, F. Schäfers, W. Gudat, O. Zaharko, H. Grimmer, and P. M. Oppeneer, "Resonant magnetic reflection coefficients at the Fe 2p edge obtained with linearly and circularly polarized soft x rays," Phys. Rev. B **66**, 184404 (2002).
[16]S. Valencia, A. Kleibert, A. Gaupp, J. Rusz, D. Legut, J. Bansmann, W. Gudat, and P. M. Oppeneer, "Quadratic x-ray magneto-optical effect upon reflection in a near-normal-incidence configuration at the M edges of 3d-transition metals," Phys. Rev. Lett. **104**, 187401 (2010).
[17]E. Hecht, *Optics* (Addison Wesley, 2002).
[18]D. Kim, Y.-W. Oh, J. U. Kim, S. Lee, A. Baucour, J. Shin, K.-J. Kim, B.-G. Park, and M.-K. Seo, "Extreme anti-reflection enhanced magneto-optic Kerr effect microscopy," Nat. Commun. **11**, 5937 (2020).
[19]C. Jin, Z. Tao, K. Kang, K. Watanabe, T. Taniguchi, K. Mak, and J. Shan, "Imaging and control of critical fluctuations in two-dimensional magnets," Nat. Mater. **19**, 1290–1294 (2020).
[20]J. F. Dillon, Jr., H. Kamimura, and J. P. Remeika, "Magneto-optical properties of ferromagnetic chromium trihalides," J. Phys. Chem. Solids **27**, 1531–1549 (1966).
[21]J. F. Dillon, Jr., "Origin and uses of the Faraday rotation in magnetic crystals," J. Appl. Phys **39**, 922 (1968).
[22]B. Kuhlow and M. Lambeck, "Magnetic domain structures in $CrBr_3$," Phys. B+C **80**, 365–373 (1975).
[23]T. Guillet, A. Marty, C. Vergnaud, F. Bonell, and M. Jamet, "Electrical detection of magnetic circular dichroism: Application to magnetic microscopy in ultrathin ferromagnetic films," Phys. Rev. Appl. **15**, 014002 (2021).
[24]C. von Korff Schmising, B. Pfau, M. Schneider, C. M. Günther, M. Giovannella, J. Perron, B. Vodungbo, L. Müller, F. Capotondi, E. Pedersoli, N. Mahne, J. Lüning, and S. Eisebitt, "Imaging ultrafast demagnetization dynamics after a spatially localized optical excitation," Phys. Rev. Lett. **112**, 217203 (2014).
[25]S. Zayko, O. Kfir, M. Heigl, M. Lohmann, M. Sivis, M. Albrecht, and C. Ropers, "Ultrafast high-harmonic nanoscopy of magnetization dynamics," arXiv:2011.05450 (2020).
[26]In dark-field microscopy, the sample is illuminated with light that will not be collected by the objective lens so that only scattered light contributes to the image formation. This produces an almost black background image with bright objects superimposed.
[27]Z. J. Yang and M. R. Scheinfein, "Combined three-axis surface magneto-optical Kerr effects in the study of surface and ultrathin-film magnetism," J. Appl. Phys. **74**, 6810 (1993).
[28]G. S. Krinchik and V. A. Artem'ev, "Magnetooptical properties of Ni, Co, and Fe in the ultraviolet, visible, and infrared parts of the spectrum," Sov. Phys. JETP **26**, 1080–1085 (1968); available at https://nam12.safelinks.protection.outlook.com/?url=http%3A%2F%2Fwww.jetp.ac.ru%2Fcgi-bin%2Fdn%2Fe_026_06_1080.pdf&data=04%7C01%7CPublication%40aippublishing.org%7C31d45323dbad4877b4ed08d93d5155f6%7Cdc10e84a5061494682799dd51547c7e9%7C0%7C0%7C637608242414169011%7CUnknown%7CTWFpbGZsb3d8eyJWIjoiMC4wLjAwMDAiLCJQIjoiV2luMzIiLCJBTiI6Ik1haWwiLCJXVCI6Mn0%3D%7C1000&sdata=9SQw128fLRqnNCK0BTw%2B9VBJDh6ZYbnoDHFmeg3%2B1Ik%3D&reserved=0.
[29]J. McCord, H. Brendel, A. Hubert, and S. Parkin, "Hysteresis and domains in magnetic multilayers," J. Magn. Magn. Mater. **148**, 244–246 (1995).
[30]P. Büscher and L. Reimer, "Imaging and colour coding of magnetic domains by Kerr scanning optical microscopy," Scanning **15**, 123–129 (1993).
[31]W. Rave, R. Schäfer, and A. Hubert, "Quantitative observation of magnetic domains with the magneto-optical Kerr effect," J. Magn. Magn. Mater. **65**, 7–14 (1987).
[32]D. B. Dove, "Photography of magnetic domains using the transverse Kerr effect," J. Appl. Phys **34**, 2067 (1963).
[33]A. Berger and M. R. Pufall, "Generalized magneto-optical ellipsometry," Appl. Phys. Lett. **71**, 965 (1997).
[34]P. M. Oppeneer, H.-C. Mertins, and O. Zaharko, "Alternative geometries for the determination of x-ray magneto-optical coefficients," J. Phys. Condens. Matter **15**, 7803–7813 (2003).
[35]J. F. Dillon, Jr., "Observation of domains in the ferrimagnetic garnets by transmitted light," J. Appl. Phys **29**, 1286 (1958).
[36]R. Schäfer and A. Hubert, "A new magnetooptic effect related to non-uniform magnetization on the surface of a ferromagnet," Physica Status Solidi (A) **118**, 271–288 (1990).
[37]H.-C. Mertins, S. Valencia, A. Gaupp, W. Gudat, P. M. Oppeneer, and C. M. Schneider, "Magneto-optical polarization spectroscopy with soft x-rays," Appl. Phys. A **80**, 1011–1020 (2005).
[38]T. von Hofe, N. O. Urs, B. Mozooni, T. Jansen, C. Kirchhof, D. E. Bürgler, E. Quandt, and J. McCord, "Dual wavelength magneto-optical imaging of magnetic thin films," Appl. Phys. Lett. **103**, 142410 (2013).
[39]I. V. Soldatov and R. Schäfer, "Selective sensitivity in Kerr microscopy," Rev. Scient. Instr. **88**, 073701 (2017).
[40]D. Markó, I. V. Soldatov, M. Tekielak, and R. Schäfer, "Stray-field-induced Faraday contributions in wide-field Kerr microscopy and -magnetometry," J. Magn. Magn. Mater. **396**, 9–15 (2015).
[41]The 635-nm quarter-wave plate is made from mica and was obtained from Bernhard Halle Nachfl. GmbH, Berlin, Germany, and the 550-nm plate was actually a quarter-wave compensator from Carl Zeiss AG, Jena, Germany.
[42]J. Kranz and A. Hubert, "Die Möglichkeiten der Kerr-Technik zur Beobachtung magnetischer Bereiche (The potential of the Kerr technique for the observation of magnetic domains)," Z. Angew. Phys. **15**, 220–232 (1963).
[43]F. Schmidt, W. Rave, and A. Hubert, "Enhancement of magneto-optical domain observation by digital image processing," IEEE Trans. Magn. **21**, 1596–1598 (1985).
[44]MO Sensor type A (Matesy GmbH, Otto-Schott-Str. 13, Jena 07745, Germany).
[45]R. Schäfer, I. V. Soldatov, and S. Arai, "Power frequency domain imaging on Goss-textured electrical steel," J. Magn. Magn. Mater. **474**, 221–235 (2019).
[46]I. Soldatov, J. Zehner, K. Leistner, T. Kang, D. Karnaushenko, and R. Schäfer, "Advanced, Kerr-microscopy-based MOKE magnetometry for the anisotropy characterisation of magnetic films," J. Magn. Magn. Mater. **529**, 167889 (2021).

[47]I. V. Soldatov and R. Schäfer, "Advances in quantitative Kerr microscopy," Phys. Rev. B **95**, 014426 (2017).
[48]P. H. Lissberger, "Kerr magneto-optic effect in nickel-iron films. II. Theoretical," J. Opt. Soc. Am. **51**, 957–966 (1961).
[49]A. Hubert and G. Traeger, "Magneto-optical sensitivity functions of thin-film systems," J. Magn. Magn. Mater. **124**, 185–202 (1993).
[50]L. Wenzel, V. Kamberský, and A. Hubert, "A systematic first-order theory of magnetooptic diffraction in magnetic multilayers," Phys. Status Solidi A **151**, 449–466 (1995).
[51]We have started with a coated sample as antireflection coatings seemed to be an important ingredient for circular dichroism according to Ref. 18. In the meantime, we have found that with background subtraction, a similarly good contrast can as well be seen on uncoated FeSi specimens. (not shown).
[52]T. Narushima and H. Okamoto, "Circular dichroism microscopy free from commingling linear dichroism via discretely modulated circular polarization," Sci. Rep. **6**, 35731 (2016).
[53]R. Schäfer, M. Rührig, and A. Hubert, "Exploration of a new magnetization-gradient-related magnetooptical effect," IEEE Trans. Magn. **26**, 1355–1357 (1990).
[54]A. Thiaville, R. Schäfer, and A. Hubert, "An isotropic description of the new-found gradient-related magneto-optical effect (invited)," J. Appl. Phys. **69**, 4551 (1991).
[55]V. Kamberský, "The Schäfer-Hubert magneto-optical effect and classical gyrotropy in light-wave equations," J. Magn. Magn. Mater. **104–107**, 311–312 (1992).
[56]V. Kamberský and R. Schäfer, "Magneto-optic gradient effect in domain-wall images: At the crossroads of magneto-optics and micromagnetics," Phys. Rev. A **84**, 013815 (2011).
[57]H. Boersch and M. Lambeck, "Zur Beugung des Lichtes an Magnetisierungsstrukturen," Z. Phys. **177**, 157–163 (1964) (in German).
[58]M. Lambeck, "Image formation by magneto-optic effects," Optica Acta **24**, 643–655 (1977).
[59]M. Lambeck, "Zur Abbildung von Magnetisierungsstrukturen mit dem Faraday- und Kerr-effekt," Z. Phys. **179**, 161–181 (1964) (in German).